Neural coding of choice and outcome are modulated by uncertainty in orbitofrontal but not secondary motor cortex

Juan Luis Romero-Sosa[1], Alex Yeghikian[1], Andrew M. Wikenheiser[1-3], Hugh T. Blair[1-3#] & Alicia Izquierdo[1-4#]

[1]Department of Psychology, University of California-Los Angeles, Los Angeles, California, USA.

[2]The Brain Research Institute, University of California-Los Angeles, Los Angeles, California, USA.

[3]Integrative Center for Learning and Memory, University of California-Los Angeles, Los Angeles, California, USA.

[4]Integrative Center for Addictions, University of California-Los Angeles, Los Angeles, California, USA.

Author contributions:

AI: Conceptualization, methodology, formal analysis, resources, writing-original draft, writing-review & editing, software, supervision, and funding. **JLRS**: Conceptualization, methodology, formal analysis, investigation, data curation, writing- original draft preparation, writing- review & editing, software, and visualization. **AY:** Investigation, data curation, formal analysis, software, and visualization. **AMW:** Formal analysis and writing- review & editing. **HTB:** Formal analysis, resources, writing- review & editing, supervision, and funding.

Corresponding authors:

Juan Luis Romero-Sosa jromero12@ucla.edu and

Dr. Alicia Izquierdo aizquie@ucla.edu

Abstract

Orbitofrontal cortex (OFC) and secondary motor cortex (M2) are both implicated in flexible reward learning but the conditions that differentially recruit these regions are not fully understood. We imaged calcium activity from single neurons in OFC or M2 during *de novo* learning of uncertain reward probability schedules. Predictions of choice were decoded from M2 neurons with high accuracy under all certainty conditions, but were more accurately decoded from OFC neurons under greater uncertainty. In M2, the proportion of outcome-selective neurons decreased with uncertainty whereas this proportion remained stable in OFC, due to an increased recruitment of reward-selective neurons across levels of uncertainty. Decoding accuracy of both choice and outcome were predicted by indices of flexible strategy like Win-Stay and Lose-Shift in OFC, but not M2. When schedules were experienced in increasing and then decreasing uncertainty, chemogenetic perturbation of M2 and OFC neurons resulted in opposing roles in certain and uncertain conditions, respectively. Our results indicate that M2 neurons are causally involved in learning of more certain conditions, whereas OFC neurons preferentially encode choices and outcomes that foster greater reliance on adaptive strategies under conditions of uncertainty. This reveals a novel functional heterogeneity within frontal cortex in support of flexible learning.

INTRODUCTION

Both the orbitofrontal cortex (OFC) and secondary motor cortex (M2) are involved in flexible reward learning and reward-motivated decision making. M2 receives dense inputs from diverse cortices, including sensorimotor, visual, retrosplenial, and orbital regions[1], and in turn, sends projections to striatum that fall along mediolateral and rostrocaudal gradients within M2[2], enabling precise control of actions. This anatomical connectivity positions M2 well to control action flexibly based on both sensory and motivation information. Functional studies have determined that M2 is essential for action updates [3] and that it enables the flexible assignment of either stimuli or motor antecedents to action plans[4-6]. Additionally, there has been discovery of different population dynamics in M2 depending on the strategy and stimulus modality that mice use in a flexible decision-making task[7]. Given its integration of sensory and motivation evidence, M2 has an essential role in higher-order movement control and orienting [8] but can also bias choice based on outcomes and choice history[9, 10]. Though a previous electrophysiological study indicated orbitofrontal cortex (OFC) is involved in updating outcome value from prior actions[11], authors found that M2 signaled choice earlier than any other area of rat frontal cortex, and remarkably also contained a value signal[12].

OFC also has a well-substantiated role in flexible decision making[13-16]. Several groups have reported choice-predictive neurons in OFC in equivalent or even larger numbers than value or outcome-encoding cells in this region[17-21]. One group found that over half of the neurons they recorded in OFC encoded both the direction of choice and the location of the goal, concluding that choice selective neurons in OFC represent spatial-motor information required to define specific goals and necessary actions to obtain them[21]. However, it is presently unclear if and how these representations change with uncertainty. By uncertainty we mean stochasticity, or moment-to-moment probabilistic outcomes[22] generating an 'expected uncertainty'[23-25], not uncertainty resulting from volatility, or the rate of change[22]. Indeed, a somewhat parallel literature suggests OFC may be critically involved in learning, especially under uncertain or probabilistic conditions[26-28], where it may set the expectation for the rest of learning[24, 25, 29, 30]. This is consistent with the idea that OFC stores long-term action values[24, 31], stimulus values[32], and causally contributes to an expected uncertainty or baseline risk in rats[33, 34]. This risk is signaled by single neurons in OFC in rats [35, 36] and in nonhuman primates[37, 38]. One study [39] reported that OFC neurons track expectations across a slow timescale (i.e., across-session probabilistic reversal learning) and are also recruited for trial-by-trial learning, or value updates, on a fast timescale (i.e., within a session). However, this study did not manipulate the reward uncertainty over time. Critically, aside from the

Hattori et al. (2023) study, recording and imaging studies in both rodent and primate species typically assess the role of OFC in decisions in expert animals, not during the learning of risk or expected uncertainty. Thus, it is unknown how choice and outcome cell selectivity may change over the course of learning, especially with increasing uncertainty in OFC. All of the above suggests that although M2 and OFC are involved in flexible learning and decision-making, their involvement could dissociate over different timescales and increasingly uncertain conditions.

Using miniscopes, we compared populations of neurons and single cells in OFC and M2 over several sessions of learning in freely-behaving rats. Unlike the great number of studies assessing these regions in well-trained animals, here we studied calcium dynamics during *de novo* learning. We were primarily interested in determining if and when neural dynamics would differentially predict choice and outcome in M2 vs. OFC, and which behavioral and task features single cells were selective for in these regions across learning under uncertainty.

RESULTS

Learning under increasing uncertainty

Male and female Long–Evans rats first underwent stereotaxic surgery to infuse GCaMP6f into either M2 or OFC (see Methods). In the same surgery, a GRIN lens was unilaterally implanted over the site of the viral infusion (**Figure 1I-K**; photomicrographs of lens implant and calcium indicator expression for all rats are shown in **Supplementary Figure 1**). Following surgical recovery and baseplating, rats then underwent pretraining followed by six sessions of learning. In a touchscreen-outfitted chamber, rats were required to initiate each trial by touching a center stimulus and then make a choice to touch a stimulus on either the left or right side. If correct, rats could retrieve a sucrose pellet reward from a food port located on the opposite side of the touchscreen response zone, signaled by a light cue in the port. This visual cue appeared concurrently with pellet delivery on rewarded, but not unrewarded, trials. The reward contingencies reversed every 75 trials and increased in uncertainty on the last block of trials, with reward schedules progressing from less to more reward uncertainty (100:0 to 70:30) (**Figure 1A-B**). The probability of reward delivery depended on the rat's choice (left vs. right), with one side delivering a higher probability of reward than the other. Each session consisted of 3 blocks of 75 trials (225 trials total); the response with the highest reward probability (left vs. right) was reversed at the start of each block. Within each session, the probability ratio remained the same for the first two trial blocks and then changed to a ratio with higher uncertainty for the last block of trials. As shown in **Figure 1C**, sessions 1 and 2 used a ratio of 100:0 for blocks 1-2 and 90:10 for block 3

(Schedule 1), sessions 3 and 4 used a ratio of 90:10 for blocks 1-2 and 80:20 for block 3 (Schedule 2), and sessions 5 and 6 used a ratio of 80:20 for blocks 1-2 and 70:30 for block 3 (Schedule 3). **Figure 1D** shows an example of a single rat's performance during a Schedule 2 session.

Results of an omnibus Generalized Linear Model (GLM) on predictors of accuracy are found in **Table 1**. Rats tended to improve across all trials (GLM: $\beta_{trialnum} = 0.01$, $p < 0.01$) while performance expectedly dipped on block switches when reversals occurred (GLM: $\beta_{block} = -0.439$,

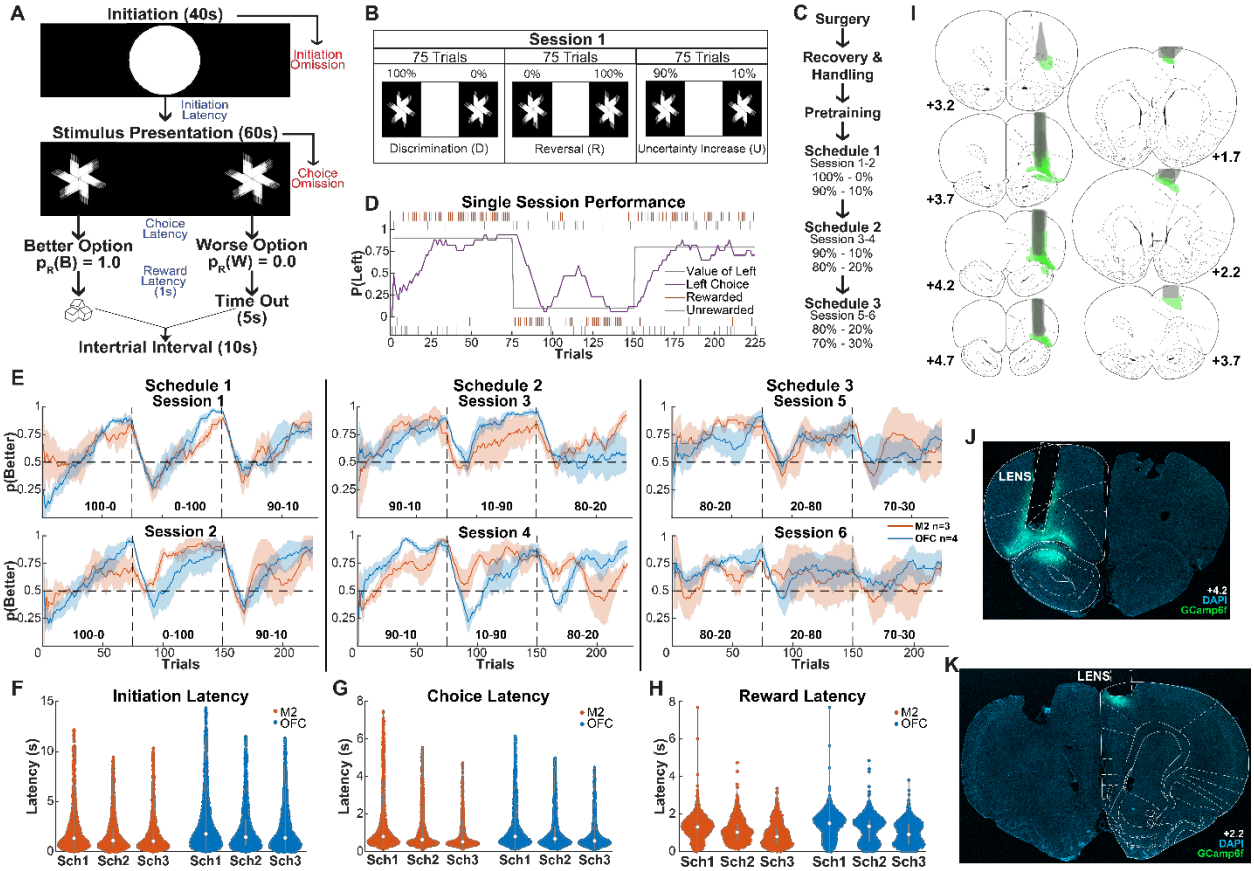

Figure 1. Probabilistic reversal learning task performance in freely-behaving, lens-implanted rats. **(A)** Schematic of trial timeline: Rats learn in an operant chamber outfitted with a touchscreen with three different interaction zones (left, center, and right) and a reward port on the opposite side of the chamber. A white circle is presented in the middle zone for 40 seconds, during which the rat is required to nosepoke to initiate a trial. Subsequently, two identical stimuli are presented on the left and right side of the screen for 60 seconds. The rat is required to nosepoke one of these stimuli, selecting either the left or right side. One of the sides has a higher reward probability than the other. The rat either gets rewarded 1 s after the nosepoke or undergoes a 5-second timeout. There is a 10 second Intertrial Interval (ITI) before a new trial begins. **(B)** A session consists of 3 blocks of 75 trials each, with two reversals, with the last block increasing in uncertainty. **(C)** Following surgery, recovery, handling, and pretraining to respond to touchscreen stimuli on either the left or the right, different schedules are introduced, with each schedule administered across two days each, and increasing in uncertainty. **(D)** Sample performance on Schedule 2 where the rat matches the value of the left side and adapts its behavior following a reversal. **(E)** There was no significant difference in accuracy, or p(Better), by lens implant area (**Table 1**). **(F-H)** Performance measures by lens implant region to include latencies for Initiation **(F)**, Choice **(G)**, and Reward **(H)** for M2- and OFC-lens implanted rats across all the schedules. **(I)** Reconstructions of calcium indicator GCaMP6f and GRIN lens implant in all rats. **(J)** Photomicrograph of a lens in OFC. **(K)** Photomicrograph of a lens in M2.

$p < 0.01$), **Figure 1E**. We found there were no significant differences in lens implant location on learning accuracy as measured by probability correct (**Table 1**).

Though rats with lens implants in M2 vs. OFC did not differ in their acquisition rates (**Table 1**), compared with a sham control group, implanted animals exhibited slightly attenuated learning compared to viral, non-tethered controls (GLM: $\beta_{Implanted_Lens} = -0.13$, $p < 0.01$, **Supplementary Figure 2, Supplementary Table 1**). For latency measures, non-tethered control animals initiated trials and collected rewards more quickly but exhibited slower choice latencies (**Supplementary Tables 2-4**). Latencies to initiate trials and collect reward did not differ in M2- vs. OFC-implanted animals, but choice latencies were faster in the OFC-implanted animals than in the M2-implanted animals (GLM: $\beta_{Area} = -0.57$, $p < 0.01$, **Figure 1F-H**, **Tables 2-4**).

Decoding choice from calcium activity

Binary support vector machine (SVM) classifiers were trained to predict *Chosen Side* (left vs. right) from calcium traces aligned to the choice nosepoke (**Figure 2A-B)**. To determine the most appropriate windows for statistical analysis, we generated peak-aligned heatmaps and found cells that exhibited time-locked activity to either choice or reward cue **(Figure 2D-E)**. Decoder training sets were balanced to include an equal number of rewarded/unrewarded and left/right trials across all schedules (**Figure 2C**). In both M2 and OFC, choice decoding accuracy ramped up from chance starting prior to trial initiation (suggesting that rats often anticipated which side they would choose prior to trial initiation), and peaked ~500 ms after choice (**Figure 2F**). An analysis of predictors of decoding accuracy in the bin just prior to choice (yellow shaded region in **Figure 2F**) resulted in more accurate decoding in M2 than OFC ($\beta_{Area} = -0.231$, $p = 0.0004$), with no effect of schedule ($\beta_{Schedule} = -0.0843$, $p = 0.19$), but a significant Area x Schedule interaction ($\beta_{Area:Schedule} = 0.056$, $p = 0.0475$), **Table 5**. *Chosen Side* was decoded from M2 with similarly high accuracy under all probability schedules, whereas decoding was more accurate in OFC when the schedule was more uncertain. Confirming this, post-hoc analyses on each schedule (**Table 6**) revealed that decoding from M2 was more accurate than from OFC under conditions of higher certainty (Schedule 1: $\beta_{Area} = -0.174$, $p = 0.0027$; Schedule 2: $\beta_{Area} = -0.119$, $p = 0.0438$), but under the least certain schedule, OFC decoding accuracy increased to become equivalent to M2 decoding accuracy (Schedule 3: $\beta_{Area} = -0.0621$, $p = 0.073$). This certainty-dependent decoding accuracy in OFC was not accounted for by experience (i.e., session) since experience was a covariate in the GLM model and was not a significant predictor of choice accuracy ($\beta_{Session} = 0.0268$, $p = 0.234$). Additionally, to check if the number of neurons used to train decoders affected decoder accuracy, we entered this variable as a moderator in the GLM. We did not find any

significant effect or interaction with any other variable ($\beta_{NumCells}$ = -0.0008, p = 0.22, $\beta_{NumCells:Area}$ = 0.0008, p = 0.12, $\beta_{NumCells:schedule}$ = 0.0004, p = 0.17, $\beta_{NumCells:Area:schedule}$ = -0.0003, p = 0.19), indicating that ensemble size did not significantly explain decoder accuracy results.

Decoding outcome from calcium activity

SVM classifiers were trained to predict *Trial Outcome* (rewarded vs. unrewarded) from calcium traces aligned to the choice nosepoke (**Figure 2A-B**). At time points before the outcome was known (that is, prior to 1 second after the choice nosepoke), the accuracy of outcome

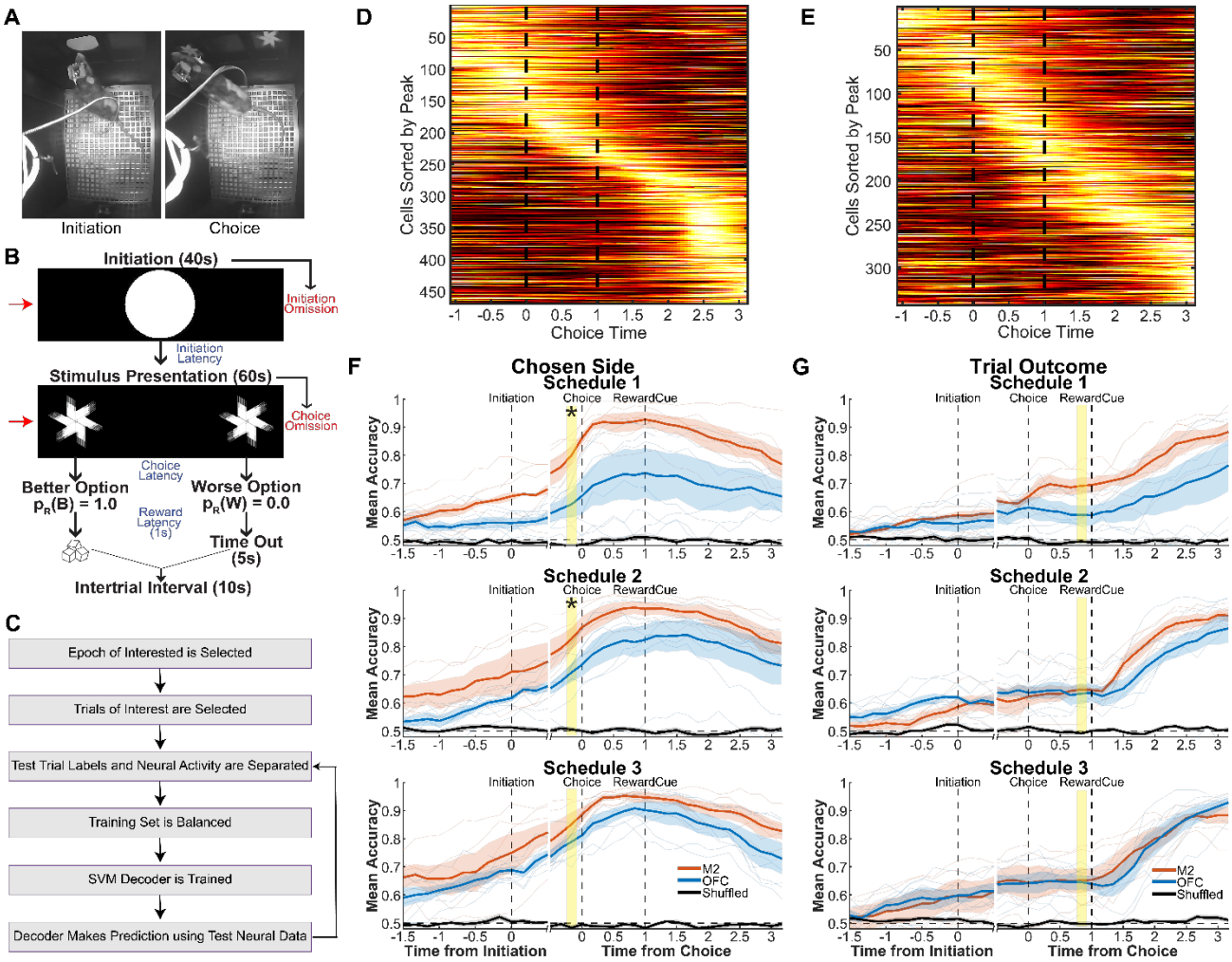

Figure 2. OFC, but not M2, choice decoding accuracy increases with uncertainty. **(A)** Trial epochs selected for analysis of neural data: Initiation (left) and Choice (right). **(B)** Same epochs in A, shown in the trial timeline. **(C)** A flowchart of how the decoder was trained with balanced data and then tested on each trial. **(D)** Example of a cross-validated peak-aligned heatmap aligned at choice from an imaging session in M2 during schedule 2. **(E)** Same as D but in OFC. **(F)** Decoder accuracy from an SVM binary decoder trained using balanced neural data from either M2 or OFC. The solid line is the mean and the shaded region is the standard deviation. The decoder was trained to predict whether the choice would be left or right (*Chosen Side*). We found a main effect of Area and Area x Schedule interaction, with post-hoc analysis revealing better decoding in M2 than OFC in Schedule 1 and 2, but not Schedule 3. Decoder accuracy using shuffled neural data in both M2 and OFC is shown in black. **(G)** Similar to F but here the decoder was trained to predict whether the trial would be rewarded or not (*Trial Outcome*). We found main effects of Area and Schedule, but no significant interaction of Area x Schedule. *p< 0.05.

decoding was limited by the certainty of the outcome (which was highest under Schedule 1 and lowest under Schedule 3). In both M2 and OFC, decoding accuracy for *Trial Outcome* began ramping up from chance at trial initiation and then stalled at a plateau which persisted until the outcome was known, after which decoding accuracy began ramping upward again (**Figure 2G**). A GLM analysis of decoding accuracy in the bin just prior to the outcome (yellow shaded region in **Figure 2G**) resulted in, as expected, better decoding of outcome for certain than uncertain schedules ($\beta_{Schedule}$ = -0.128, p = 0.0494). Decoding was also more accurate in M2 than OFC (β_{Area} = -0.138, p = 0.0248). There was similarly no effect of overall experience, or session number (**Table 7**). Here we also included the number of neurons as a moderator and again did not find a significant effect or interaction of ensemble size with any of the other predictors ($\beta_{NumCells}$ = -0.00001, p = 0.98, $\beta_{NumCells:Area}$ = 0.0002, p = 0.59, $\beta_{NumCells:schedule}$ = 0.0002, p = 0.34, $\beta_{NumCells:Area:schedule}$ = -0.0002, p = 0.31). The same analysis was conducted on only co-registered cells (i.e., the decoder was trained on session 1 and tested on session 2, within the same schedule), **Supplementary Figure 6**. This revealed a similar pattern as **Figure 2F** and pointed to greater stability for Chosen Side decoding over Trial Outcome.

The ratio of choice- and reward- selective neurons increases with uncertainty in OFC, but not in M2

To link the decoder results to single cell selectivity, we removed an increasing number of cells with large beta coefficients (**Supplementary Figure 3**). As expected, decoder accuracy steadily dropped as more neurons with the largest beta coefficients were removed. We show heatmap plots of average trial activity for neurons that were significantly selective ($p<0.05$) for *Chosen Side*, *Trial Outcome*, and *Reward Retrieval* (**Figure 3A-C**), as well as trial-by-trial raster plots of calcium activity from individual example cells (**Figure 3G-I**).

M2 contained a higher ratio of neurons selective for *Chosen Side* than OFC throughout all schedules (GLM, β_{Area} = -0.238, p < 0.01). There was a significant interaction between area and schedule (GLM, $\beta_{AreaxSchedule}$ = 0.063, p = 0.007) (**Table 8**), reflecting the fact that the ratio of choice-selective neurons increased in OFC with uncertainty (GLM, $\beta_{Schedule}$ = 0.06, p < 0.01, **Figure 3D**), but was not influenced by uncertainty in M2 (GLM, $\beta_{Schedule}$ = 0.004, p = 0.78) (**Table 9**). Session (i.e., experience) was not a significant predictor of cell selectivity. Thus, the ratio of choice-selective neurons increases in OFC with uncertainty, but does not change with uncertainty in M2.

For the *Trial Outcome* epoch, we found a significant difference in the ratio of outcome-selective cells, with M2 once again containing a higher ratio than OFC (GLM, β_{Area} = -0.14, p = 0.01). This ratio was also not modulated by experience alone as session was not a significant predictor. There was a significant interaction of area and schedule (GLM, $\beta_{AreaxSchedule}$ = 0.05, p = 0.01, **Table 10**), resulting from the fact that the ratio of outcome-predictive neurons in M2 decreased with increasing reward uncertainty (GLM, $\beta_{Schedule}$ = 0.05, p = 0.04; **Figure 3E**), whereas the ratio of outcome-predictive neurons in OFC was similar regardless of reward uncertainty (GLM, $\beta_{Schedule}$ = 0.02, p = 0.15) (**Table 11**). Since uncertain outcomes are less predictable, it is expected that the proportion of outcome-predictive neurons should decrease with increasing reward uncertainty, as observed in M2. However, it is somewhat paradoxical to observe that the proportion of neurons encoding reward outcome in OFC remains stable despite decreases in the certainty of reward. One possible explanation for this could be that under conditions of greater uncertainty, additional OFC neurons are recruited not only to encode behavioral choices (as shown above) but also to encode reward outcome. If so, then this recruitment of additional reward-selective neurons may counteract the decreased proportion of such neurons that would otherwise result from increased uncertainty (as seen in M2).

Prior evidence suggests that value integration may occur at the time of *Reward Retrieval*[29, 40-42], so we performed an additional analysis to measure the proportion of neurons that were reward-selective during a 1-s time window centered on head entry into the reward port during rewarded trials versus a corresponding time window from unrewarded trials (see Methods). There was a larger percentage of reward-selective cells in M2 compared to OFC (GLM, β_{Area} = -0.27, p = 0.02) with a significant Area by Schedule interaction (GLM, $\beta_{AreaXSchedule}$ = 0.1, p = 0.03) (**Table 12**), resulting from the fact that OFC exhibited a higher proportion of reward-selective neurons for schedules with greater uncertainty (GLM, $\beta_{Schedule}$ = 0.09, p = 0.026, **Figure 3F**), whereas M2 showed a similar percentage of reward-selective neurons across all schedules (GLM, $\beta_{Schedule}$ = -0.01, p = 0.44). Again, it is an increase in uncertainty and not experience (**Table 13**) that drives this increase in the ratio of reward-selective cells in OFC, since session was once again not a predictor of cell selectivity.

218

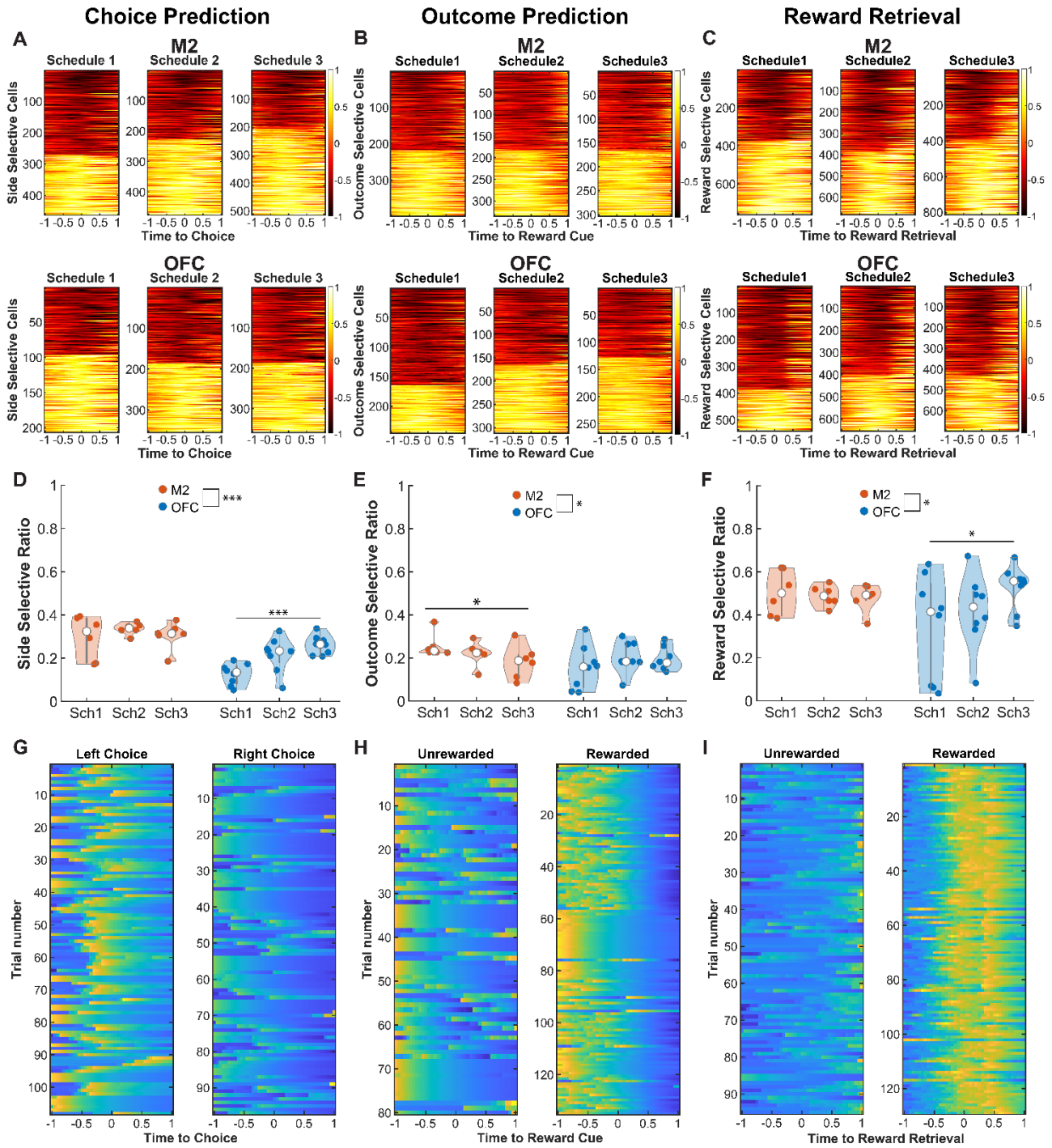

Figure 3. Decoder results are explained by changes in the ratio of selective cells across schedules. **(A)** Each row plots the difference in trial averaged activity of left trials minus right trials triggered by the time of choice. Cells plotted are all imaged neurons where we observed a significant effect of side, sorted from most negative beta coefficient to most positive one. The activity of the neurons was range-normalized. A value closer to 1 indicates more selectivity for the left side trials and a value closer to -1 indicates more selectivity for the right side. **(B,C)** Same as A but the difference is averaged activity of unrewarded trials minus rewarded trials, centered at time of reward cue (B) or reward retrieval (C). **(D)** Ratio of side selective neurons is overall larger in M2 but it increases with schedule only in OFC. **(E)** Ratio of outcome selective neurons is overall larger in M2 and decreases with uncertainty only in M2. **(F)** Ratio of reward selective neurons is overall larger in M2 but increases with schedule only in OFC. **(G)** Example of the z-score normalized activity of a significant side-selective M2 neuron on left and right trials. **(H)** Same as G but for a significant outcome-selective M2 cell. **(I)** Same as G but for a significant reward-selective OFC neuron. *p<0.05. ***p<0.001.

Behavioral strategies predict decoding accuracy in OFC, not in M2

To assess the degree to which different behavioral measures (**Figure 4A-F**) modulated decoding accuracy in OFC and M2, we analyzed the data using an omnibus mixed-effects GLM for *Chosen Side* (**Table 14**) and *Trial Outcome* (**Table 16**). As predictors, we included primary behavioral measures described above such as median initiation, choice, and reward latencies for the entire session (**Figure 4I-K**), as well as secondary measures such as Win-Stay (WS, proportion of trials when the rat repeated a response for which it had been rewarded on the previous trial) and Lose-Shift (LS, proportion of trials when the rat did not repeat a response for which it had been unrewarded on the previous trial), which we and others have previously used to assess adaptive strategies in both stimulus and action-based learning[24, 43]. As other predictors, we included a Flexibility Index (see Methods) that measured the animal's ability to adapt to trial block reversals, and a Perseveration Index, or the mean number of trials to shift choice behavior after being unrewarded, divided by the number of first unrewarded trials[44].

We found significant M2 vs. OFC area interaction effects for Win-Stay, Lose-Shift, and Perseveration Index in the bin just before the choice epoch (**Figure 4H**, **Table 14**). Post-hoc GLMs revealed that only initiation latencies (GLM: $\beta_{InitiationLatency} = -0.067$, $p = 0.0324$) significantly predicted *Chosen Side* decoder accuracy for M2 (**Figure 4I**, **Table 15**). In contrast, WS (GLM: $\beta_{WinStay} = 0.843$, $p = 0.0008$) and LS (GLM: $\beta_{LoseShift} = 1.466$, $p = 0.0240$) positively predicted, whereas Perseveration Index (GLM: $\beta_{Perserveration\ Index} = -4.128$, $p < 0.0001$) negatively predicted *Chosen Side* decoder accuracy in OFC (**Figure 4J**, **Table 15**). Similar post-hoc GLMs (**Figure 4K**, **Table 16**) found no significant behavioral predictors for *Trial Outcome* decoding accuracy in M2 (**Figure 4L, Table 17**), but again found that WS (GLM: $\beta_{WinStay} = 0.652$, $p = 0.0202$) and LS (GLM: $\beta_{LoseShift} = 1.550$, $p = 0.0228$) positively predicted and Perseveration Index (GLM: $\beta_{Perserveration\ Index} = -1.543$, $p = 0.0498$) negatively predicted *Trial Outcome* decoding accuracy in OFC (**Figure 4M, Table 17**). These analyses indicate that complex, strategy-level behaviors contribute to decoding accuracy in OFC, but not M2.

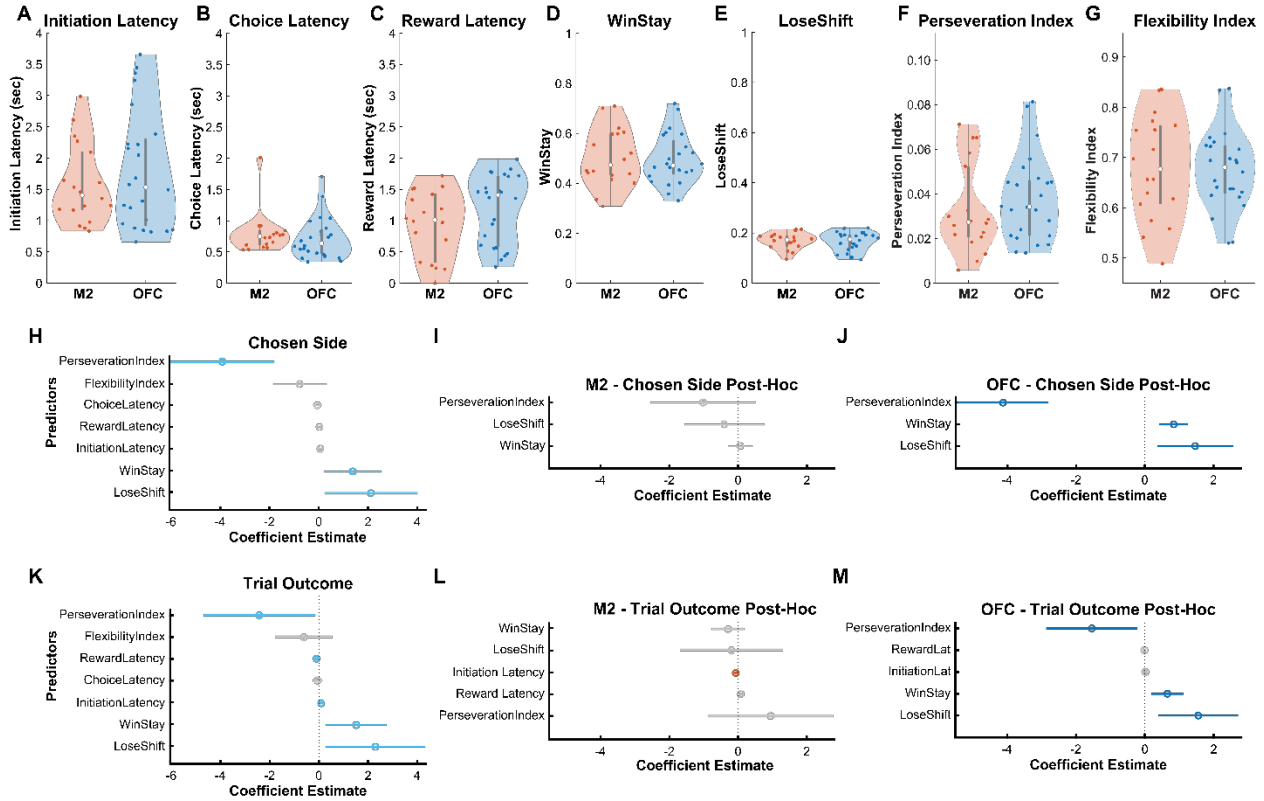

Figure 4. Chosen Side and Trial Outcome decoding accuracy is predicted by behavioral strategy only in OFC. **(A-G)** Behavioral measurements that were entered as regressors in omnibus Generalized Linear Models (GLM). Latency measures **(A-C)** were calculated as medians of all trials for each session. WinStay and LoseShift **(D-E)** were calculated as the proportion of total trials that were WinStay and LoseShift at the session level. Perserveration Index and Flexibility Index **(F-G)** were calculated using formulas described in the Methods. **(H)** Beta coefficients for regressors where significant area (M2 vs. OFC) interactions were found in predicting decoder accuracy of *Chosen Side*. Modeling was performed only on the accuracy from the bin right before choice (highlighted in yellow, Figure 2) **(I)** Post-Hoc GLM performed on sessions from rats with lenses in M2. **(J)** Post-Hoc GLM performed on sessions from rats with lenses in OFC. Strategy indices were significant predictors of *Chosen Side* decoding accuracy in OFC, but not in M2. **(K)** Beta coefficients for regressors where significant area (M2 vs. OFC) interactions were found in predicting *Trial Outcome*. Similarly, to H, analyses were only performed on the bin before reward cue (highlighted in yellow, Figure 2). **(L)** Post-Hoc GLM performed on sessions from rats with lenses in M2. **(M)** Post-Hoc GLM performed on sessions from rats with lenses in OFC. Strategy indices were significant predictors of *Trial Outcome* decoding accuracy in OFC, but not in M2.

OFC, but not M2, neurons preferentially support adaptive learning in uncertain conditions

Male and female Long-Evans rats underwent stereotaxic surgery to infuse hM4Di DREADDs in either OFC or M2 (see Methods). After following the same pretraining scheme as rats with lens implants, this cohort performed schedules first in order of increasing uncertainty (identical to the cohort with lens implants) and then in order of decreasing uncertainty (which rats with lens implants did not experience). Each schedule was administered twice- with CNO

inhibition on the first session and an injection of vehicle (VEH) on the second session- before the rat advanced to the next schedule (**Figure 5A**).

Data were analyzed by computing the percentage of correct trials within a 15-trial window that was advanced across the trials on each session (see Methods). We show frequency histograms for the proportion of correct trials per window (**Figure 5B**), collapsed within each session type (**Figure 1B**). We analyzed the percentage of correct trials per window with omnibus GLMs (**Tables 18 and 20)**, finding no significant effect of session in any of the analyses; thus, sessions within the same schedule were collapsed. Block reversals were once again found to be associated with decreases in accuracy in both OFC (GLM: $\beta_{Block} = -0.408$, $p < 0.001$) and M2 cohorts (GLM: $\beta_{Block} = -0.379$, $p < 0.001$). Task accuracy was impaired by OFC inhibition across all schedules, with the largest effect size in Schedule 3 (GLM: $\beta_{CNO} = -0.059$, $p < 0.001$). However, M2 inhibition impaired performance only in Schedule 1 (GLM: $\beta_{CNO} = -0.039$, $p < 0.001$) (**Figure 5B**). Indeed, M2 inactivation only affects learning on the more certain schedule regardless of whether it appeared first or last, whereas OFC inactivation affects performance on the first session, and following that, with effect sizes that scale with uncertainty (**Supplementary Figure 7**). These results indicate the inhibition of OFC is associated with learning deficits across levels of uncertainty, while M2 is only affected under more deterministic conditions.

We then analyzed the impact of inhibition of these regions on Win-Stay and Lose-Shift strategies (**Tables 22-27**). OFC inhibition decreased Win-Stay across all schedules (GLM: $\beta_{CNO} = -0.020$, $p < 0.01$). Interestingly, M2 inhibition decreased Win-Stay only in Schedules 1 and 2, with the effect size decreasing with uncertainty. While OFC inhibition did not affect Lose-Shift, M2 inhibition increased Lose-Shift only in Schedule 2 (**Figure 5D**).

Finally, we assessed initiation, choice, and reward latencies following inhibition (**Figure 5C**), finding more variable effects (**Tables 28-37**). Both M2 and OFC inhibition resulted in faster initiation latencies across all schedules. OFC inhibition resulted in slower choice latencies in Schedules 1 and 2 and faster choice latencies in Schedule 3, while M2 inhibition resulted in faster choice latencies in Schedules 1 and 2 only. Reward latencies were increased following OFC inhibition across all schedules, whereas M2 inhibition resulted in decreased reward latency for Schedule 1 and increased reward latency for Schedule 2. Only animals with confirmed, well-targeted bilateral expression were included in all analyses (**Figure 5E-F**).

285

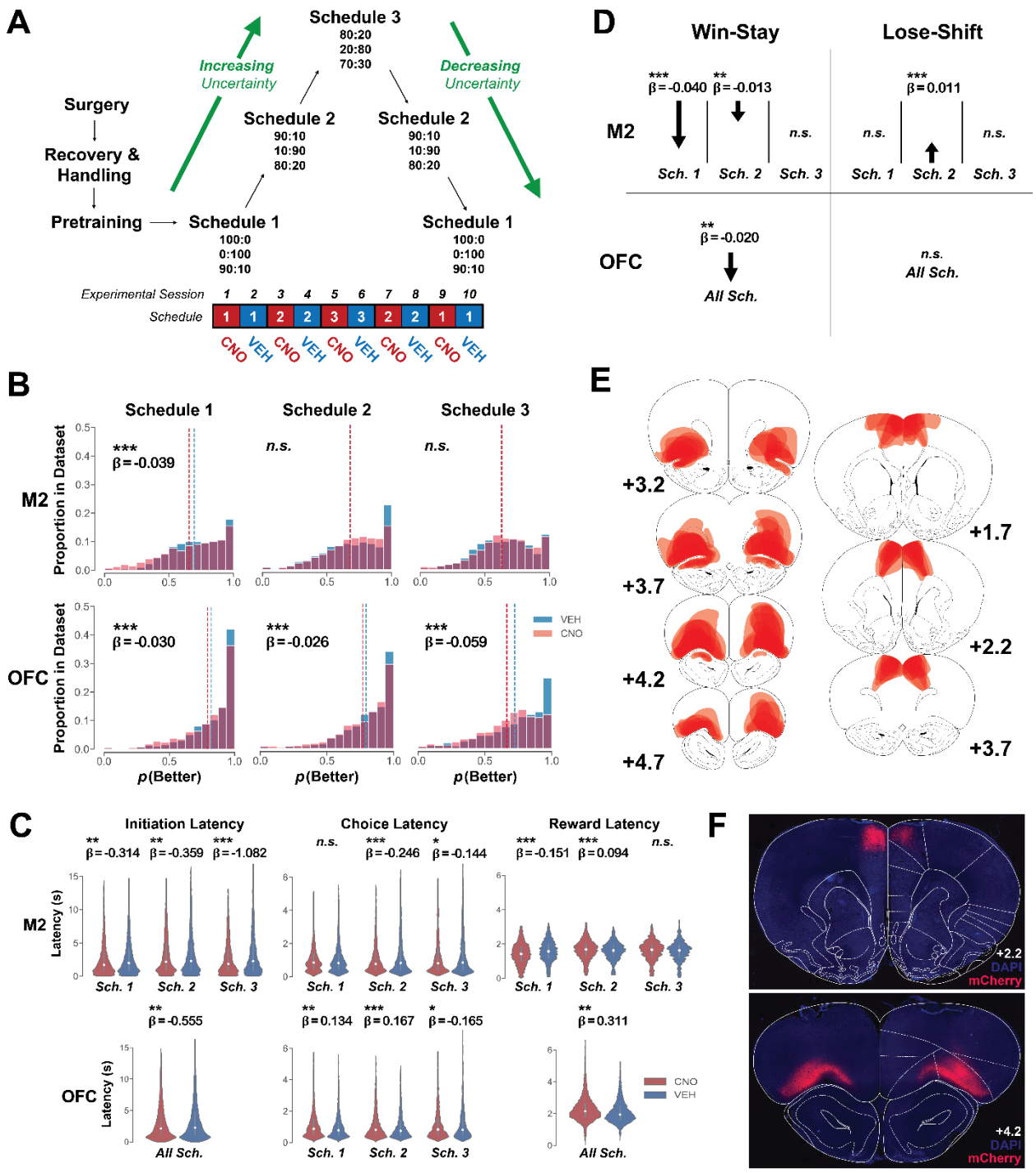

Figure 5. DREADDs inhibition of OFC and M2 neurons produces dissociable effects in learning under uncertainty and certainty, respectively. **(A)** Following surgery, recovery, handling, and pretraining rats were introduced to different schedules, first in increasing order of uncertainty followed by decreasing (reverse) order. Each schedule was administered across two days, the first under CNO inhibition and the second following an injection of vehicle (VEH). **(B)** As there was no effect of session, we collapsed schedules across learning. OFC inhibition resulted in attenuated accuracy, with the largest effect size of inhibition in the most uncertain schedule. In contrast, attenuated accuracy was observed following M2 inhibition in only the schedule with the most certainty. Beta coefficients are provided for each schedule. **(C)** Inhibition of OFC and M2 resulted in distinct and varied effects on initiation, choice, and reward latencies. **(D)** Win-stay behavior was reduced across all schedules by OFC inhibition and only in the two schedules with least uncertainty by M2 inhibition. Lose-shift behavior increased in Schedule 2 under M2 inhibition. **(E)** Reconstructions of DREADD expression across all rats. **(F)** Representative photomicrographs of hM4Di-mCherry DREADD expression in M2 and OFC. *p<0.05, **p<0.01, ***p<0.001.

DISCUSSION

We imaged single-cell activity in M2 and OFC while freely-moving rats underwent learning. Using a binary support vector machine decoder, we found evidence of functional heterogeneity in frontal cortex at both the population- and single-cell level. Specifically, M2 consistently contained more information about choice on individual trials than OFC, yet decoder accuracy increased with uncertainty, not just experience, only in OFC, not M2. We found that decoder accuracy was predicted by adaptive strategies in OFC, but not M2. We also determined that M2 and OFC neurons exhibited different neural trajectories in learning trial types: these changed dynamically in more uncertain schedules in OFC, but not M2 (**Supplementary Figure 4**). Our single cell analyses revealed a recruitment of an increasing ratio of choice- and reward- selective neurons in OFC with uncertainty, not M2. Finally, chemogenetic inactivation of each of these regions confirmed functional roles for OFC, but not M2, as preferentially involved in learning under uncertainty. Collectively, these results suggest that neurons in OFC are more engaged in conditions with higher task demands that require adaptive strategies, such as increased uncertainty during learning.

There are several novel and confirmatory findings here. First, studies of neural activity in the frontal cortex in mice[45], rats[46, 47], and especially non-human primate subjects [48] typically involve extensive training prior to surgery to ensure that the animal is a task expert prior to any recording or imaging. In contrast, in the present experiment, rats learned the task *de novo* while we imaged single cells from these regions, which allowed us to determine that the dynamics in OFC changed as the uncertainty increased. Quite differently, M2 signaling of choice was robust and stable throughout the experiment. With the exception of two single-unit electrophysiological studies[11, 12], these two brain regions have not been systematically compared for their signaling in a reward-motivated task until now, and importantly, the previous studies administered a dynamic foraging task where subjects were not required to learn any task structure. We used a similar task to that in a recent report by Hattori and colleagues[39], but those authors also did not vary the uncertainty in the reward environment, as we did here. Consistent with their findings, we confirm that OFC plasticity is required for 'across session' learning (what authors call "meta-learning"), and here we extend this to conditions of increasing uncertainty encoded in OFC, but not in M2, neurons.

Studies following manipulations in rat OFC in flexible reward learning have included targeting the entire ventral surface [49, 50] or comparisons of medial vs. lateral OFC[27, 28]. Similar to a recent study using identical targeting[24], here we examined the role of ventrolateral OFC, a subregion not as often probed as medial and more lateral OFC[51], and found evidence consistent

with its encoding of expected uncertainty[25]. Specifically, several studies using different methods [32-34, 52] suggest OFC must be 'online' to establish a baseline risk associated with probabilistic outcomes from which to gauge meaningful changes (i.e., reversals or block switches). OFC-inhibited animals also do not employ effective Win-Stay strategies[24], consistent with the GLM modeling results of the imaging experiment and the causal chemogenetic perturbation result.

Here we find evidence that OFC neurons learn task structure details that are ultimately useful in predicting the consequences of decisions in uncertain and/or novel conditions[53]. In support of this, we found that OFC neurons do not encode choices as well during more certain schedules, evidenced in both decoder and stability analyses where M2 decoder accuracy is greater than that of OFC in the more certain schedules. Additionally, we observed an increase in the proportion of neurons that signaled reward with increasing uncertainty in OFC, not in M2. These findings are consistent with the idea that OFC has a pivotal role in creating a task map[54, 55]: just as a spatial map helps one move better through space, a task map would help with adaptive behavioral strategies. We show evidence of this with decoder performance in OFC positively predicted by adaptive strategies WinStay, LoseShift, and negatively correlated with an inflexibility measure like Perseveration Index.

By comparison to OFC, M2 is often overlooked in learning studies due to its presumed stronger role in motor skill and action execution in both rodents and non-human primates[56-58]. There is evidence that M2 encodes task-relevant features, such as whether a rat will choose the left or right side in a bandit task [12] and a risky or safe option[59]. Thus, our results provide additional evidence that M2 encodes important task parameters such as choice and trial outcome. Even with recruitment of a decreasing proportion of outcome-selective cells with uncertainty (**Figure 3E**), this change ultimately had not impact on decoding accuracy of trial outcome in M2. Indeed, M2 is relatively unchanging: its encoding of choice remained robust and dynamics in this region contained a "full picture" of task-relevant features even from the initial phases of learning. In support of this, we found that M2 contained information related to blocks throughout all different epochs of a trial, more so than OFC **(Supplementary Figure 5)**. Additionally, chemogenetic inactivation of M2 preferentially impacts learning in more deterministic conditions, as evidenced by the lower accuracy and poorer Win-Stay strategy in less uncertain schedules. Given that M2 biases decision-making processes[5, 10], an early read-out of “intention” could be a useful brain-machine interface application, given its stable coding.

These findings demonstrate distinct roles for M2 and OFC in processing task-specific information during learning under uncertainty, with M2 neurons maintaining robust, stable activity

throughout learning, and OFC neurons exhibiting significant adaptations in response to uncertainty. This suggests a mechanism by which OFC neurons make adjustments to dynamic environments, while M2 provides a more consistent response control mechanism. Interestingly, unlike the present findings that suggest a role for rodent OFC in both outcome and reward probability encoding, primate OFC is not as important for encoding of reward "availability, as indexed by its probability"[60]. Instead, OFC is more specialized in primates for value and "desirability," not probability. This may be an important primate-rodent difference to consider when interpreting experimental findings in frontal cortex across species in the future.

Acknowledgements

This work was supported by NIH 2R01DA047870, NSF NeuroNex 1707408, and NIH F31MH135698. We thank the members of the Izquierdo and Wikenheiser labs for their feedback and suggestions. We would also like to thank the members of Romero Sosa's dissertation committee, Drs. Kate Wassum and Dean Buonomano, for their feedback on experimental design. Finally, we thank Dr. Dmitriy Lisitsyn for help setting up the CaImAn pipeline and Dr. Alireza Soltani for his valuable feedback on analyses and interpretation.

METHODS

Subjects

A total of N=32 Long-Evans rats was used. Subjects for single-cell calcium imaging were n=7 adult Long-Evans rats: n=4 (3 males, 1 female) with lenses in OFC and n=3 (2 females, 1 male) with lenses in M2. Subjects for chemogenetic manipulation were N=25 adult Long-Evans rats. Of these, seven animals were excluded from analyses: one due to a failure to complete pretraining and six due to weak or unilateral viral expression. Thus, the total for the chemogenetic experiment was N=18: OFC: n=9, 5 females; M2: n=9, 5 females. Rats were obtained from a colony of GAD-Cre transgenic rats (RRRC#751; Rat Resource and Research Center, MO) / TH-Cre (RRRC#659; Rat Resource and Research Center, MO), genotyped as wildtype. Rats were pair-housed when they arrived at our housing facilities and then single-housed after undergoing surgery. Rats were housed in plastic transparent tubs filled with bedding media made of wood shavings in a room with a reverse 12-hour light cycle. Pretraining and testing occurred during their dark period, seven days per week until all experimental sessions were completed. Motivation was

383 achieved through a progressive food restriction until the weight was kept above 85% of their initial
384 free-feeding weight. Rats had free access to water at all times. Before training, rats were handled
385 for 10-20 min for a minimum of 5 consecutive days. Subsequently, rats were introduced to a three-
386 finger hold that enabled intraperitoneal injections or the attachment of a miniscope after
387 baseplating. Experiments were conducted with the approval of, and following the guidelines
388 established by, the Chancellor's Animal Research Committee at UCLA.

389 **Behavioral Pretraining**

390 Our operant chambers were outfitted with a touchscreen on one end, divided into three
391 zones (left, center, and right), and a reward port opposing the touchscreen (Models 80604 and
392 80604A, Lafayette Instrument, Inc., Lafayette, IN). Ten sucrose pellets were placed in the rat's
393 homecage one day before training to acclimate them to the pellets. The rats were placed in the
394 operant chambers on the first training day, and 5 pellets were dispensed. The rats remained in
395 the chambers for 20 min, where they could explore, eat the pellets, and become habituated to the
396 testing environment. The criterion for the rat to move on to the next phase is eating all 5 pellets
397 within the allotted time. The following day, they begin Initial Touch Center (ITC), which was the
398 first time the rat had learned to interact with the touchscreen. A trial commenced with the display
399 of a white rectangle in the center zone to indicate the rat is required to interact with it (e.g., nose
400 poke or paw touch). Once the rat interacted with the center zone, a pellet was immediately
401 delivered to the reward port. The rat only had 40 s to interact with the center zone before the
402 rectangle disappeared, and the trial was counted as an initiation omission. If the rat successfully
403 interacted with the center zone and collected the sucrose pellet, the trial was considered a
404 committed trial. For the rat to move on from ITC, it had to complete 60 committed trials within 45
405 min. The final phase of pretraining was Immediate Reward (IR). In this phase, the rat was required
406 to initiate the trial by touching the center zone when the white rectangle is presented, and then it
407 was required to touch a stimulus presented pseudo randomly either on the left or right zone of the
408 touchscreen. The rat had 60 s to interact with this stimulus to obtain a reward. Similar to the ITC
409 criterion, for the rat to complete IR, it had to complete 60 committed trials within 45 min. After
410 completing IR, rats were considered ready for surgery.

411 **Miniscope Assembly and Imaging**

412 We purchased assembled Miniscope V4.4 kits from *Open Ephys*. The miniscope was
413 placed in a 3D-printed, custom-designed, and constructed helmet (a link to the 3D design would
414 be excellent here). The 3D-printed helmet enabled us to utilize a more resilient SMA connector

415 for rat movement. Once the miniscope was fitted inside the helmet, we ensured LED power, the
416 electrowetting lens, and the CMOS were working correctly. The tether used to connect the
417 miniscope to the operating system had a female SMA connector on one end and a male HDMI
418 connector on the opposite end. A motorized commutator from Doric Lenses (Part Number:
419 AERJ_24_HDMI+4) allowed the tether to rotate with the rat. The commutator transferred the
420 signal to the miniscope DAQ v3.3, also obtained from *Open Ephys*. The DAQ sent the signal over
421 USB to a recording computer. Additionally, the DAQ produced a TTL pulse every time the
422 miniscope recorded a frame of data. These TTL pulses were recorded in parallel with TTL pulses
423 sent by the operant chamber whenever certain behaviors within a trial were performed (i.e., trial
424 initiation, reward port entry) and were used to time lock neural data to specific epochs within trials
425 and within single sessions. These TTL pulses were recorded using a CerePlex Direct data
426 acquisition system and later used to sync the neural data. The USB signal from the miniscope
427 was recorded onto a Framework Laptop 13 (11th Gen Intel) using the Miniscope DAQ Software
428 (build v1_11). All imaging was conducted at a rate of 20 frames-per-second (fps).

429 **GCaMP and Lens Implant Surgeries**

430 Rats were anesthetized with isoflurane (5% induction, 2% maintenance in 2.5 L/min O_2)
431 and placed in a stereotaxic apparatus (Kopf Instruments, Tujunga, CA). After clearing the skull,
432 we leveled the skull by ensuring the difference in DV around bregma was not greater than 0.05
433 mm. An etchant was applied to the skull for 1 min to ensure the adhesive would adhere. After
434 cleaning the etchant, we partially drilled seven tiny holes that would be used for seven anchor
435 screws (Fine Science Tools #19010-00). Two anchor screws were placed in the very front, two
436 directly posterior from bregma, two anterior to lambda, and one contralateral to where the GRIN
437 lens would be placed. Subsequently, a 1.2 mm diameter craniotomy was drilled above the brain
438 regions of interest. For OFC placement, the coordinates were AP: +3.7mm, ML: +2.5mm, and for
439 M2 placement, the coordinates were AP: +2.0mm, ML: +0.7mm. The craniotomy was cleaned to
440 ensure that the superior sagittal sinus was intact, and then the dura was carefully removed. A 1μL
441 Hamilton syringe and pump delivered GCaMP6f (AVV9-CamKII-GCaMP6f-WPRE-SV40,
442 Addgene, # 100834) through cannulae and injectors in either OFC or M2. For OFC surgeries, we
443 unilaterally infused virus into two different sites (AP: +3.7mm, ML: +2.5mm, DV: −4.2mm
444 and −4.6mm). For M2, we also infused unilaterally into two different sites (AP: +2.0mm, ML:
445 +0.7mm, DV: −1.4mm and −0.9mm). We dialed down 0.05mm more ventrally in either region to
446 create a pocket for infusions. We then injected 0.5μL of GCaMP6f per site, thus totaling 1μL of
447 virus per surgery. The syringe was placed in a Hamilton pump with a speed of 0.1μL per minute.

448 Following each infusion, 5 min elapsed before the cannula was moved. Lens implantation
449 occurred immediately after viral infusions. A 23-gauge needle was attached to the stereotaxic
450 instrument, zeroed at bregma, and then lowered to make clear a path for the lens. Next, the lens
451 was lowered to the halfway point between the DV coordinates as above using a vacuum. After
452 the GRIN (Gradient Index) lens had been placed in its location, we used viscous Loctite super
453 glue to glue the sides of the lens to the top of a dry skull, then added a layer of Metabond bone
454 cement that coats the lens, anchor screws, and the most superficial layer of the skull. After
455 allowing 5-10 min for the Metabond to dry, we poured opaque dental dement on the Metabond to
456 fully cover the anchor screws and cover the sides of (but not obscure) the GRIN lens. Before the
457 dental cement thoroughly dried, we affixed a custom 3D-printed lens cover. After drying the dental
458 cement, we applied a layer of topical antibiotic to the edge of the dental cement head cap. Animals
459 were administered carprofen (5mg/kg s.c.) and saline (1cc) prior to completion of surgery. Post-
460 operative care consisted of carprofen (5mg/kg s.c.) for five days following surgery.

461 We waited 3 to 4 weeks post-surgery to allow for GCaMP expression before attaching the
462 baseplate. We anesthetized the rat for baseplating, removed the lens protector, and cleaned the
463 top of the dental cement head cap. We attached a baseplate to a fully assembled miniscope using
464 a custom 3D holder. We lowered the miniscope and the baseplate until we could focus entirely
465 on the top of the implanted GRIN lens, searching for visible expression in the area of interest,
466 then fixing the baseplate using dental cement. GCaMP expression and lens implant
467 reconstructions are shown for OFC (**Figure 1D, left**) and for M2 (**Figure 1D, right**), along with
468 representative photomicrographs (**Figure 1E-F**)**.** All GCaMP and lens placements for all animals
469 are shown in **Supplementary Figure 1**.

470 **Viral Surgeries**

471 Craniotomies were performed similarly to the GCaMP surgeries. To express inhibitory
472 hM4Di DREADDs (Designer Receptors Exclusively Activated by Designer Drug) in cortical
473 excitatory neurons, a CaMKIIα promoter drove the hM4Di-mCherry sequence (Addgene viral prep
474 # 50477-AAV8, Watertown, MA). This construct was infused bilaterally into either OFC or M2 at
475 the same coordinates as previously described. 0.5μL was infused per site, thus totaling 1μL per
476 hemisphere and 2μL per surgery. The scalp was carefully closed using self-dissolving sutures to
477 ensure a fast and less invasive recovery.

Experimental testing began a minimum of three weeks after surgery to allow for receptor expression. Reconstructions of DREADD expression are shown for OFC (**Figure 5D, left**) and for M2 (**Figure 5D, right**), along with representative photomicrographs (**Figure 5C**).

Behavioral Testing

After the baseplating surgery, rats were again put on food restriction before behavioral testing: they were eased into a restricted diet over three days to no more than 85% of their free-feeding weight. Additionally, rats were once again habituated to a gentle hold and plugging the miniscope into the baseplate. Rats were given a second round of pretraining as an acclimating imaging session using a miniscope. We ensured rats performed many trials in the IR phase (> 200 trials in 45 mins) before moving the rat onto the main behavioral task.

Learning of Probabilistic Reversals. Similar to pretraining, a trial began when a circle was displayed in the center zone of the touchscreen. The rat must interact with it by nose-poking or touching it with its paw within 40 s; otherwise, it is scored as an initiation omission. After touching the circle, two identical stimuli were presented on both the right and left touchscreen zones. The rat had to interact with either the left or the right zones. The rat had 60 s to make a choice otherwise, it was scored as a choice omission. One of the zones was associated with a higher probability of reward, while the other was associated with a lower probability of reward. If the rat received a sucrose pellet reward, it was dispensed in the reward port on the opposite side of the chamber, and the subsequent trial began after a 10-s inter-trial interval (ITI). If the rat did not receive a reward, a 5-s time-out was imposed in addition to the 10-s ITI. If the rat initiated a trial and made a choice within the allotted time, the trial was scored as a committed trial regardless of whether it was rewarded. Food motivation was assessed purely by the number of committed trials, not accuracy. In each session, there were three blocks of 75 committed trials each.

From one block to the next, the location of the highest-valued side reversed. The probability of each option itself varied by block according to schedule, with Schedule 1 including deterministic blocks (100:0, 0:100, 90:10) and Schedules 2 (90:10, 10:90, 80:20) and 3 (20:80, 80:20, 70:30) being entirely probabilistic. There was an increase in uncertainty over testing. There were two primary reasons for this design: 1) reversals (i.e., block design) keep the animals engaged and less likely to fall into a motor habit of always responding left, for example, and 2) we enhance the chance of including the same cell population during learning at one level of uncertainty (e.g., 100-0) with another (90-10), if these blocks occur in the same session. Task structure is visualized in **Figure 1A**. Violin plots for all initiation, choice, and reward latencies are

510 shown by schedule (**Figure 1I-K**), and the median per session collapsed across all schedules for
511 each of these groups.

512 *Chemogenetic inhibition*. In the chemogenetic cohort (n=18), inhibition of OFC or M2 was
513 achieved with systemic administration of clozapine-N-oxide, CNO (6 mg/kg, i.p., in 95% saline,
514 5% DMSO; HelloBio, Princeton, NJ) 30 min prior to behavioral testing. To control for the
515 nonspecific effects of injection and handling, vehicle solution, VEH (95% saline, 5% DMSO), was
516 alternatively administered. The effects of CNO were assessed in a within-subjects design where
517 rats completed each schedule twice, first under CNO administration and second with an injection
518 of VEH. To investigate learning in changing environments while controlling for the effect of task
519 experience in navigating the task, rats first completed the schedules in increasing order of
520 uncertainty, then repeated these schedules in decreasing order **(Figure 5A).**

521 **Histology**

522 Following completion of behavioral testing, all rats were euthanized with an intraperitoneal
523 dose of sodium pentobarbital and sodium phenytoin (Euthasol® Euthanasia Solution) and
524 transcardially perfused with PBS and a 4% formalin solution. Brains were extracted, placed in 4%
525 formalin solution for at least 24 h, and subsequently left in a 30% sucrose solution for at least 24
526 h. Forty µm coronal sections were mounted onto slides and coverslipped with DAPI to visualize
527 GCaMP or hM4Di-mCherry expression. Imaging was performed using a LSM 900 confocal
528 microscope (Zeiss) and BZ-X710 florescence microscope (Keyence).

529 **Post-processing calcium imaging pipeline**

530 Miniscope recording videos were processed using custom Python code and the Python
531 version of CaImAn[61]. We concatenated videos and cropped them to focus the field of view (FOV)
532 with the neural activity. We then passed it through the motion correction algorithm in CaImAn,
533 with the central parameter *gSif_filt* set between 6 and 12 for our data. All of the motion correction
534 for our data was conducted with the piece-wise rigid motion correction Boolean setting set to true.
535 We performed the non-rigid algorithm if this algorithm did not fix the motion artifacts. Once the
536 motion correction was completed, the motion-corrected videos were passed on to the CNMF-E
537 portion of CaImAn[61]. The main parameters we used for the CNMF-E were as follows: the half size
538 of a neuron = 8; the half size of the neuron's bounding box = 16; for every session, we chose a
539 value to separate the first and most significant population of minimum peak-to-noise (PNR) ratio
540 resulting in use of a range between 7-16; for the minimum correlation value we found values
541 between 0.75 and 0.85 worked best. Every other setting was left to CaImAn default. After CNMF-

E, we performed a component analysis. We set the Boolean parameter *use_cnn* to true so that CaImAn would use a trained convolution-neural network (CNN) model to assign a value between 0-1 that determined how close the components matched the appearance of soma. The algorithm used three different values to determine if a component should be as accepted as a cell: Spatial footprint consistency (*rval*), Signal-to-Noise ratio (*snr*), and CNN threshold value (*cnn_thr*), with the minimum values for each of these set to 2.5, 0.85, and 0.85, respectively. We then visually-inspected random components. Since, according to CaImAn documentation, it is not advised to calculate deltaF/F when using 1P data (due to the inability to confidently calculate baseline with background activity) we used the function *estimates.detrend_df_f* with the flag *detrend_only* set to true to calculate fluorescence where baseline has been subtracted but has not been normalized by it. Additional settings used were: quantileMin = 8, frames_window = 250, use_residuals = True. Finally, we calculated the deconvolved traces of the accepted components using the CaImAn function *estimates.deconvolve*. This removed any change in the fluorescence not due to the dynamics of the neurons. After the detrended and deconvolved values were calculated, all of the outputs were saved into a .mat file (MATLAB, MathWorks Inc., Natick, MA), for all further processing. In MATLAB, we combined the output from CaImAn with TTL pulses to align activity of neurons around specific epochs of behavior.

Some of the videos had banding artefact caused by a known issue with the USB controller of the UCLA miniscope DAQ. When banding occurred, we first saved the frames in which this occurred and then filled the frames with the last reliable frame before the banding. Following processing with CaImAn, we replaced the data from those frames with NaNs.

Data Analysis

All data analyses were conducted using custom-written code in MATLAB.

Learning and Performance. The probability of choosing the better option was the primary measure of interest, and secondarily Initiation Latency, Choice Latency, and Reward Latency were each analyzed with a series of mixed-effects General Linear Models (GLMs) (*fitglme* function; Statistics and Machine Learning Toolbox) first with omnibus analyses that included lens group (M2-implanted, OFC-implanted). Follow-up GLMs were conducted pending significant interactions in the omnibus models. The coding of variables for GLM were: 0=females, 1=males, 0=OFC-implanted, and 1=M2-implanted). Statistical significance for GLM analyses was noted as p-values of less than 0.05. The variable of interest p(Better) was calculated starting with a boolean vector where 1s corresponded to a choice for the better option: 1 with the higher probability of

reward and a 0 for the worse option. This boolean vector was then inputted into the matlab function *movmean* where the kernel was set to [15 0]. The Win-Stay and Lose-Shift values presented in Figure 5D and Tables 22-27 were calculated similarly to p(Better). A boolean vector was generated for the entire session: 1 if the trial was Win-Stay / Lose-Shift and 0 if it was not. These boolean vectors were then inputted into *movmean* to generate a proportion of trials within this window that were Win-Stay or Lose-Shift. The following are definitions of predictors: *TrialNum*: The number of trials within an entire session (from 1 to 255); *Session*: Experimental day (from 1-6 in the calcium imaging and 1-10 in the DREADDs experiment); *Block*: The number of blocks within a single session (from 1-3); *Area*: The brain area for calcium imaging (1=M2, 0=OFC); *Schedule*: The uncertainty schedule (from 1-3). The remaining predictors are defined in the Results section.

Cross Validated Peak-Aligned Heatmap. A window of detrended fluorescence 1 s before and 3 s after choice was obtained for every trial in a session. This resulted in a matrix of cell-by-frame-by-trial averaged across all trials for a resulting cell-by-frame matrix. This was normalized using the normalize function on Matlab with the 'range' parameter. The max in a cell's activity was 1, and the minimum was 0 to ensure fair comparison across all cells in that session. The odd trials of neurons were then peak aligned and the resulting indices were used to plot the even trials using *imagesc*. Vertical dashed bars show the moment of choice and the moment of reward cue.

Decoder Analysis. A 4-s window of detrended fluorescence centered around Initiation was obtained for every trial in a session. Separately, another 4-s window (1-s before and 3-s after) of detrended fluorescence around choice was obtained for every trial in a session. This resulted in a cell-by-frame-by-trial matrix for initiation and a separate one for choice. We temporally downsampled so that activity in bin 1 was the average of frames 1-6, activity in bin 2 was the average of frames 3-9, and so on. Every trial was also labeled as either a left or right choice, whether rewarded or unrewarded (win or lose). One trial was left out for testing the decoder, and the rest of the trials were then balanced so that there would be the same number of left-rewarded, left-unrewarded, right-rewarded, and right-unrewarded conditions across all sessions in training of the decoder. The balanced trials were randomly selected for every test trial to sample the entire dataset of trials per session. Once the balanced subset of trials was selected, the neural data for that session and the labels were inputted into the Matlab function *fitcsvm* with the "KernelFunction" set to 'linear.' The decoder was then tested on the neural data for the test trial, and the result was tallied as a 1 if the label matched the test label and a 0 if it was mismatched. This was conducted for every single trial in a session. Additionally, we reran the decoder on all

trials per session, but with the trial type labels randomly shifted. This data is shown as "Shuffled" in **Figure 2F-G**. Statistical comparisons and post-hocs were performed using Matlab's *fitglme* function, and the formulas are included in the corresponding tables. Accuracy measures from the bin (average of 5 frames) before choice were utilized for the *Chosen Side* GLMs and accuracy measures before the reward cue were used for the *Trial Outcome* GLM.

Single Cell Selectivity GLM. Activity for every neuron was obtained on the same bins used for the GLMs for decoder accuracy. In addition to *Chosen Side* and *Trial Outcome* activity, we used the averaged activity 5 frames before and after *Reward Retrieval* for single cell selectivity analysis. Statistics were conducted using Matlab's *fitglme* and the formulas for γ = neural activity were γ ~ [1 + side] for Chosen Side and γ ~ [1 + rewarded] for both Trial Outcome and Reward Retrieval. After a GLM was fitted for every cell per session, the ratio of selective cells (ones with a p-value lower than 0.05) was obtained. We then fit GLM models to the ratios across both areas and all three schedules. The Beta coefficients used for **Supplementary Figure 3** were optained from the same GLMs used to obtain these ratios. They are also from the same time bins as **Figure 2F-G** and the Reward Retrieval timepoint described above.

Behavioral measurements. Latencies were recorded from ABET in Lafayette Instrument chambers. Initiation latency measured the time from the presentation of the white circle on the center touch zone until a rat interacts with the middle zone. Choice latency measured the time from the presentation of both stimuli to the time the rat interacts with one of the stimuli to make a choice. Reward latency measures the time from the dispensed pellet until the rat enters the reward port to retrieve the pellet. WinStay was calculated as the percentage of all trials when the rat received a reward on the previous trial and chose the same side for the following trial. LoseShift was calculated as the percentage of all trials when the rat did not receive a reward and chose a different side for the subsequent trial. The Perseveration Index was calculated as the average number of trials to change choice after being unrewarded. Flexibility Index was calculated as follows:

$$FlexIndex = mean[(mean(C_{Better}\text{Block1}, C_{Better}\text{Block2}), (mean(C_{Better}\text{Block2}, C_{Better}\text{Block3})]$$

where C_{Better} is equal to 1 if the animal chose the better option and 0 otherwise, with the better option defined according to the reward schedule for each block. Statistical comparisons and post-hocs were performed using Matlab's *fitglme* function, and the formulas are included in the corresponding tables. Accuracy measures from the bin before choice were utilized for the *Chosen*

638 *Side* GLMs and accuracy measures from the bin before the reward cue were used for the *Trial*
639 *Outcome* GLM.

640 **REFERENCES**

641 1. Reep, R.L., G.S. Goodwin, and J.V. Corwin, *Topographic organization in the corticocortical*
642 *connections of medial agranular cortex in rats.* J Comp Neurol, 1990. **294**(2): p. 262-80.
643 2. Reep, R.L. and J.V. Corwin, *Topographic organization of the striatal and thalamic connections of*
644 *rat medial agranular cortex.* Brain Res, 1999. **841**(1-2): p. 43-52.
645 3. Gremel, C.M. and R.M. Costa, *Premotor cortex is critical for goal-directed actions.* Front Comput
646 Neurosci, 2013. **7**: p. 110.
647 4. Barthas, F. and A.C. Kwan, *Secondary Motor Cortex: Where 'Sensory' Meets 'Motor' in the Rodent*
648 *Frontal Cortex.* Trends Neurosci, 2017. **40**(3): p. 181-193.
649 5. Murakami, M., et al., *Neural antecedents of self-initiated actions in secondary motor cortex.* Nat
650 Neurosci, 2014. **17**(11): p. 1574-82.
651 6. Ostlund, S.B., N.E. Winterbauer, and B.W. Balleine, *Evidence of action sequence chunking in goal-*
652 *directed instrumental conditioning and its dependence on the dorsomedial prefrontal cortex.* J
653 Neurosci, 2009. **29**(25): p. 8280-7.
654 7. Siniscalchi, M.J., et al., *Fast and slow transitions in frontal ensemble activity during flexible*
655 *sensorimotor behavior.* Nature Neuroscience, 2016. **19**(9): p. 1234-1242.
656 8. Erlich, J.C., M. Bialek, and C.D. Brody, *A cortical substrate for memory-guided orienting in the rat.*
657 Neuron, 2011. **72**(2): p. 330-43.
658 9. Ebbesen, C.L., et al., *More than Just a "Motor": Recent Surprises from the Frontal Cortex.* J
659 Neurosci, 2018. **38**(44): p. 9402-9413.
660 10. Yang, J.H. and A.C. Kwan, *Secondary motor cortex: Broadcasting and biasing animal's decisions*
661 *through long-range circuits.* Int Rev Neurobiol, 2021. **158**: p. 443-470.
662 11. Sul, J.H., et al., *Distinct roles of rodent orbitofrontal and medial prefrontal cortex in decision*
663 *making.* Neuron, 2010. **66**(3): p. 449-60.
664 12. Sul, J.H., et al., *Role of rodent secondary motor cortex in value-based action selection.* Nat
665 Neurosci, 2011. **14**(9): p. 1202-8.
666 13. Tsuchida, A., B.B. Doll, and L.K. Fellows, *Beyond reversal: a critical role for human orbitofrontal*
667 *cortex in flexible learning from probabilistic feedback.* J Neurosci, 2010. **30**(50): p. 16868-75.
668 14. Gardner, M.P. and G. Schoenbaum, *The orbitofrontal cartographer.* Behavioral neuroscience,
669 2021. **135**(2): p. 267.
670 15. Rudebeck, P.H. and E.A. Murray, *The orbitofrontal oracle: cortical mechanisms for the prediction*
671 *and evaluation of specific behavioral outcomes.* Neuron, 2014. **84**(6): p. 1143-56.
672 16. Izquierdo, A., et al., *The neural basis of reversal learning: An updated perspective.* Neuroscience,
673 2017. **345**: p. 12-26.
674 17. Zhou, J., et al., *Prospective representations in rat orbitofrontal ensembles.* Behav Neurosci, 2021.
675 **135**(4): p. 518-527.
676 18. Campos, M., et al., *Orbitofrontal cortical activity during repeated free choice.* Journal of
677 Neurophysiology, 2012. **107**(12): p. 3246-3255.
678 19. Kimmel, D.L., et al., *Value and choice as separable and stable representations in orbitofrontal*
679 *cortex.* Nature Communications, 2020. **11**(1): p. 3466.
680 20. Luk, C.H. and J.D. Wallis, *Choice coding in frontal cortex during stimulus-guided or action-guided*
681 *decision-making.* J Neurosci, 2013. **33**(5): p. 1864-71.

21. Feierstein, C.E., et al., *Representation of Spatial Goals in Rat Orbitofrontal Cortex.* Neuron, 2006. **51**(4): p. 495-507.
22. Piray, P. and N.D. Daw, *A model for learning based on the joint estimation of stochasticity and volatility.* Nat Commun, 2021. **12**(1): p. 6587.
23. Woo, J.H., et al., *Mechanisms of adjustments to different types of uncertainty in the reward environment across mice and monkeys.* Cogn Affect Behav Neurosci, 2023. **23**(3): p. 600-619.
24. Aguirre, C.G., et al., *Dissociable Contributions of Basolateral Amygdala and Ventrolateral Orbitofrontal Cortex to Flexible Learning Under Uncertainty.* J Neurosci, 2024. **44**(2).
25. Soltani, A. and A. Izquierdo, *Adaptive learning under expected and unexpected uncertainty.* Nat Rev Neurosci, 2019. **20**(10): p. 635-644.
26. Dalton, G.L., et al., *Multifaceted Contributions by Different Regions of the Orbitofrontal and Medial Prefrontal Cortex to Probabilistic Reversal Learning.* J Neurosci, 2016. **36**(6): p. 1996-2006.
27. Hervig, M.E., et al., *Dissociable and Paradoxical Roles of Rat Medial and Lateral Orbitofrontal Cortex in Visual Serial Reversal Learning.* Cerebral Cortex, 2019. **30**(3): p. 1016-1029.
28. Verharen, J.P.H., et al., *Modulation of value-based decision making behavior by subregions of the rat prefrontal cortex.* Psychopharmacology, 2020. **237**(5): p. 1267-1280.
29. Young, J.J. and M.L. Shapiro, *The orbitofrontal cortex and response selection.* Ann N Y Acad Sci, 2011. **1239**: p. 25-32.
30. Keiflin, R., et al., *The orbitofrontal cortex as part of a hierarchical neural system mediating choice between two good options.* Journal of Neuroscience, 2013. **33**(40): p. 15989-15998.
31. Groman, S.M., et al., *Orbitofrontal Circuits Control Multiple Reinforcement-Learning Processes.* Neuron, 2019. **103**(4): p. 734-746 e3.
32. Namboodiri, V.M.K., et al., *Single-cell activity tracking reveals that orbitofrontal neurons acquire and maintain a long-term memory to guide behavioral adaptation.* Nat Neurosci, 2019. **22**(7): p. 1110-1121.
33. Jenni, N.L., G. Rutledge, and S.B. Floresco, *Distinct Medial Orbitofrontal-Striatal Circuits Support Dissociable Component Processes of Risk/Reward Decision-Making.* J Neurosci, 2022. **42**(13): p. 2743-2755.
34. Stolyarova, A. and A. Izquierdo, *Complementary contributions of basolateral amygdala and orbitofrontal cortex to value learning under uncertainty.* Elife, 2017. **6**.
35. Jo, S. and M.W. Jung, *Differential coding of uncertain reward in rat insular and orbitofrontal cortex.* Sci Rep, 2016. **6**: p. 24085.
36. Riceberg, J.S. and M.L. Shapiro, *Orbitofrontal cortex signals expected outcomes with predictive codes when stable contingencies promote the integration of reward history.* Journal of Neuroscience, 2017. **37**(8): p. 2010-2021.
37. O'Neill, M. and W. Schultz, *Coding of Reward Risk by Orbitofrontal Neurons Is Mostly Distinct from Coding of Reward Value.* Neuron, 2010. **68**(4): p. 789-800.
38. O'Neill, M. and W. Schultz, *Risk Prediction Error Coding in Orbitofrontal Neurons.* The Journal of Neuroscience, 2013. **33**(40): p. 15810-15814.
39. Hattori, R., et al., *Meta-reinforcement learning via orbitofrontal cortex.* Nat Neurosci, 2023. **26**(12): p. 2182-2191.
40. Izquierdo, A., R.K. Suda, and E.A. Murray, *Bilateral Orbital Prefrontal Cortex Lesions in Rhesus Monkeys Disrupt Choices Guided by Both Reward Value and Reward Contingency.* The Journal of Neuroscience, 2004. **24**(34): p. 7540-7548.
41. Ostlund, S.B. and B.W. Balleine, *Orbitofrontal Cortex Mediates Outcome Encoding in Pavlovian But Not Instrumental Conditioning.* The Journal of Neuroscience, 2007. **27**(18): p. 4819-4825.
42. Schoenbaum, G., et al., *A new perspective on the role of the orbitofrontal cortex in adaptive behaviour.* Nature Reviews Neuroscience, 2009. **10**(12): p. 885-892.

43. Harris, C., et al., *Unique features of stimulus-based probabilistic reversal learning.* Behav Neurosci, 2021. **135**(4): p. 550-570.
44. Brigman, J.L., et al., *Pharmacological or genetic inactivation of the serotonin transporter improves reversal learning in mice.* Cereb Cortex, 2010. **20**(8): p. 1955-63.
45. Bari, B.A., et al., *Stable Representations of Decision Variables for Flexible Behavior.* Neuron, 2019. **103**(5): p. 922-933.e7.
46. Hart, E.E., M.P.H. Gardner, and G. Schoenbaum, *Anterior cingulate neurons signal neutral cue pairings during sensory preconditioning.* Current Biology, 2022. **32**(3): p. 725-732.e3.
47. Constantinople, C.M., et al., *Lateral orbitofrontal cortex promotes trial-by-trial learning of risky, but not spatial, biases.* eLife, 2019. **8**: p. e49744.
48. Padoa-Schioppa, C. and J.A. Assad, *The representation of economic value in the orbitofrontal cortex is invariant for changes of menu.* Nature Neuroscience, 2008. **11**(1): p. 95-102.
49. Izquierdo, A., *Functional Heterogeneity within Rat Orbitofrontal Cortex in Reward Learning and Decision Making.* J Neurosci, 2017. **37**(44): p. 10529-10540.
50. Izquierdo, A., et al., *Basolateral amygdala lesions facilitate reward choices after negative feedback in rats.* J Neurosci, 2013. **33**(9): p. 4105-9.
51. Zimmermann, K.S., et al., *Memory Retention Involves the Ventrolateral Orbitofrontal Cortex: Comparison with the Basolateral Amygdala.* Neuropsychopharmacology, 2018. **43**(2): p. 373-383.
52. K Namboodiri, V.M., et al., *Relative salience signaling within a thalamo-orbitofrontal circuit governs learning rate.* Current Biology, 2021. **31**(23): p. 5176-5191.e5.
53. Rudebeck, Peter H. and Elisabeth A. Murray, *The Orbitofrontal Oracle: Cortical Mechanisms for the Prediction and Evaluation of Specific Behavioral Outcomes.* Neuron, 2014. **84**(6): p. 1143-1156.
54. Wikenheiser, A.M. and G. Schoenbaum, *Over the river, through the woods: cognitive maps in the hippocampus and orbitofrontal cortex.* Nat Rev Neurosci, 2016. **17**(8): p. 513-23.
55. Costa, K.M., et al., *The role of the lateral orbitofrontal cortex in creating cognitive maps.* Nat Neurosci, 2023. **26**(1): p. 107-115.
56. Alaverdashvili, M. and I.Q. Whishaw, *Motor cortex stroke impairs individual digit movement in skilled reaching by the rat.* European Journal of Neuroscience, 2008. **28**(2): p. 311-322.
57. LAWRENCE, D.G. and H.G.J.M. KUYPERS, *THE FUNCTIONAL ORGANIZATION OF THE MOTOR SYSTEM IN THE MONKEY1: I. THE EFFECTS OF BILATERAL PYRAMIDAL LESIONS.* Brain, 1968. **91**(1): p. 1-14.
58. Whishaw, I.Q., *Loss of the innate cortical engram for action patterns used in skilled reaching and the development of behavioral compensation following motor cortex lesions in the rat.* Neuropharmacology, 2000. **39**(5): p. 788-805.
59. Bao, C., et al., *The rat frontal orienting field dynamically encodes value for economic decisions under risk.* Nature Neuroscience, 2023. **26**(11): p. 1942-1952.
60. Rudebeck, P.H., et al., *Specialized Representations of Value in the Orbital and Ventrolateral Prefrontal Cortex: Desirability versus Availability of Outcomes.* Neuron, 2017. **95**(5): p. 1208-1220 e5.
61. Giovannucci, A., et al., *CaImAn an open source tool for scalable calcium imaging data analysis.* eLife, 2019. **8**: p. e38173.

TABLE 1

Across all Blocks in all Sessions for Rats with Lens Implants **γ = Percent Better Option**							
Formula	γ~[1+Session*Block*TrialNum*Area+(1+Session*Block*TrialNum|RatID)]						
Coefficients	**β**	SE	tStat	DF	P	CIL	CIU
Intercept	0.8401	0.1821	4.6124	9434	<0.0001	0.4831	1.1971
TrialNum	0.0066	0.0025	2.5965	9434	**0.0094**	0.0016	0.0115
Session	-0.0075	0.3257	-0.0230	9434	0.9817	-0.6459	0.6309
Area	-0.0724	0.2409	-0.3005	9434	0.7638	-0.5447	0.3999
Block	-0.4390	0.0876	-5.0140	9434	**<0.0001**	-0.6106	-0.2674
TrialNum:Session	-0.0007	0.0027	-0.2641	9434	0.7917	-0.0060	0.0046
TrialNum:Area	0.0044	0.0033	1.3035	9434	0.1924	-0.0022	0.0109
Session:Area	0.0483	0.4308	0.1121	9434	0.9107	-0.7962	0.8928
TrialNum:Block	-0.0001	0.0020	-0.0543	9434	0.9567	-0.0041	0.0039
Session:Block	0.0488	0.0733	0.6657	9434	0.5056	-0.0949	0.1926
Area:Block	-0.0773	0.1158	-0.6672	9434	0.5046	-0.3043	0.1498
TrialNum:Session:Area	-0.0010	0.0036	-0.2744	9434	0.7838	-0.0080	0.0060
TrialNum:Session:Block	0.0000	0.0013	-0.0309	9434	0.9753	-0.0025	0.0025
TrialNum:Area:Block	-0.0010	0.0027	-0.3801	9434	0.7039	-0.0063	0.0043
Session:Area:Block	-0.0129	0.0970	-0.1331	9434	0.8941	-0.2031	0.1773
TrialNum:Session:Area:Block	0.0003	0.0017	0.2017	9434	0.8401	-0.0030	0.0036

Alpha Level 0.05.

TABLE 2

Across all Blocks in all Sessions Comparing Lens Rats

γ = Initiation Latency

Formula	γ~[1+Session*Block*TrialNum+Area+(1+Session*Block*TrialNum|RatID)]						
Coefficients	**β**	SE	tStat	DF	P	CIL	CIU
(Intercept)	5.7688	1.5593	3.6996	9441	0.0002	2.7123	8.8254
TrialNum	-0.0450	0.0147	-3.0611	9441	**0.0022**	-0.0737	-0.0162
Session	-0.2227	0.2056	-1.0833	9441	0.2787	-0.6257	0.1803
Area	-0.4731	0.3832	-1.2344	9441	0.2171	-1.2242	0.2781
Block	0.0716	0.8186	0.0874	9441	0.9303	-1.5330	1.6762
TrialNum:Session	0.0053	0.0027	2.0071	9441	**0.0448**	0.0001	0.0105
TrialNum:Block	0.0114	0.0048	2.3661	9441	**0.0180**	0.0020	0.0209
Session:Block	-0.1536	0.1565	-0.9820	9441	0.3261	-0.4603	0.1530
TrialNum:Session:Block	-0.0010	0.0008	-1.2089	9441	0.2267	-0.0026	0.0006

Alpha Level 0.05

TABLE 3

Across all Blocks in all Sessions Comparing Lens Rats

γ = Choice Latency

Formula	γ~[1+Session*Block*TrialNum+Area+(1+Session*Block*TrialNum|RatID)]						
Coefficients	**β**	SE	tStat	DF	P	CIL	CIU
(Intercept)	2.0249	0.6468	3.1304	9441	0.0018	0.7569	3.2928
TrialNum	-0.0085	0.0065	-1.3061	9441	0.1916	-0.0213	0.0043
Session	0.0307	0.2050	0.1498	9441	0.8810	-0.3712	0.4326
Area	-0.5705	0.1600	-3.5666	9441	**0.0004**	-0.8840	-0.2569
Block	0.6944	0.4989	1.3920	9441	0.1640	-0.2835	1.6724
TrialNum:Session	-0.0006	0.0022	-0.2781	9441	0.7809	-0.0048	0.0036
TrialNum:Block	-0.0004	0.0032	-0.1219	9441	0.9030	-0.0066	0.0058
Session:Block	-0.1717	0.1449	-1.1843	9441	0.2363	-0.4558	0.1125
TrialNum:Session:Block	0.0008	0.0007	1.0717	9441	0.2839	-0.0006	0.0022

Alpha Level 0.05.

TABLE 4

Across all Blocks in all Sessions Comparing Lens Rats

γ = Reward Latency

Formula	γ~[1+Session*Block*TrialNum+Area+(1+Session*Block*TrialNum|RatID)]						
Coefficients	**β**	SE	tStat	DF	P	CIL	CIU
(Intercept)	1.5710	0.4575	3.4336	5809	0.0006	0.6740	2.4679
TrialNum	-0.0024	0.0032	-0.7300	5809	0.4654	-0.0087	0.0040
Session	-0.0524	0.0695	-0.7539	5809	0.4509	-0.1887	0.0839
Area	-0.3749	0.2199	-1.7047	5809	0.0883	-0.8060	0.0562
Block	0.2466	0.2591	0.9518	5809	0.3413	-0.2613	0.7545
TrialNum:Session	0.0002	0.0005	0.4166	5809	0.6770	-0.0008	0.0012
TrialNum:Block	-0.0002	0.0017	-0.0989	5809	0.9212	-0.0036	0.0032
Session:Block	-0.0540	0.0441	-1.2253	5809	0.2205	-0.1405	0.0324
TrialNum:Session:Block	0.0001	0.0003	0.2610	5809	0.7941	-0.0005	0.0007

Alpha Level 0.05

TABLE 5

Comparing Chosen Side Decoder Accuracy Across all Schedules in M2 and OFC **γ = Decoder Accuracy before Choice**							
Formula	γ~[1+Area*Schedule+Session+(1|RatID:Session)]						
Coefficients	**β**	SE	tStat	DF	P	CIL	CIU
(Intercept)	1.0210	0.0983	10.389	37	<0.0001	0.8219	1.2202
Area	-0.2312	0.0593	-3.9013	37	**0.0004**	-0.3513	-0.1111
Session	0.0268	0.0222	1.2109	37	0.2336	-0.0181	0.0718
Schedule	-0.0843	0.0633	-1.3307	37	0.1914	-0.2126	0.0440
Area:Schedule	0.0562	0.0274	2.0500	37	**0.0475**	0.0007	0.1118

Alpha Level 0.05**.**

TABLES 6 (Table 5 Post-Hoc)

Comparing Chosen Side Decoder Accuracy Across Schedules 1 ONLY in M2 and OFC **γ = Decoder Accuracy before Choice in Schedule 1**							
Formula	γ~[1+Area+(1|RatID:Session)]						
Coefficients	**β**	SE	tStat	DF	P	CIL	CIU
(Intercept)	0.9752	0.0661	14.755	12	<0.0001	0.8312	1.1192
Area	-0.1746	0.0401	-4.3533	12	**0.0009**	-0.2620	-0.0872

Comparing Chosen Side Decoder Accuracy Across Schedules 2 ONLY in M2 and OFC **γ = Decoder Accuracy before Choice in Schedule 2**							
Formula	γ~[1+Area+(1|RatID:Session)]						
Coefficients	**β**	SE	tStat	DF	P	CIL	CIU
(Intercept)	0.9503	0.0747	12.7138	12	<0.0001	0.787	1.113
Area	-0.1195	0.0454	-2.6330	12	**0.0219**	-0.218	-0.021

Comparing Chosen Side Decoder Accuracy Across Schedules 3 ONLY in M2 and OFC **γ = Decoder Accuracy before Choice in Schedule 3**							
Formula	γ~[1+Area+(1|RatID:Session)]						
Coefficients	**β**	SE	tStat	DF	P	CIL	CIU
(Intercept)	0.9140	0.0522	17.5113	12	<0.0001	0.800	1.028
Area	-0.0621	0.0317	-1.9613	12	0.0735	-0.131	0.007

Alpha Level 0.05.

TABLE 7

Comparing Trial Outcome Decoder Accuracy Across all Schedules in M2 and OFC **γ = Decoder Accuracy before Reward Cue**							
Formula	γ~[1+Area*Schedule+Session+(1|RatID:Session)]						
Coefficients	**β**	SE	tStat	DF	P	CIL	CIU
(Intercept)	0.8561	0.0976	8.7707	37	<0.0001	0.6583	1.0539
Area	-0.1378	0.0589	-2.3405	37	**0.0248**	-0.2571	-0.0185
Session	0.0300	0.0220	1.3612	37	0.1817	-0.0146	0.0746
Schedule	-0.1278	0.0629	-2.0321	37	**0.0494**	-0.2552	-0.0004
Area:Schedule	0.0482	0.0273	1.7686	37	0.0852	-0.0070	0.1034

Alpha Level 0.05.

TABLE 8

Comparing the Ratio of Side Selective Neurons Across all schedules in M2 and OFC **γ = Ratio of Side Selective Neurons**							
Formula	γ~[1+Area*Schedule+Session+(1|RatID)]						
Coefficients	**β**	SE	tStat	DF	P	CIL	CIU
(Intercept)	0.5512	0.0824	6.6895	37	<0.0001	0.3843	0.7182
Session	0.0208	0.0179	1.1569	37	0.2547	-0.0156	0.0571
Schedule	-0.0999	0.0512	-1.9501	37	0.0588	-0.2037	0.0039
Area	-0.2375	0.0497	-4.7775	37	**<0.0001**	-0.3383	-0.1368
Area:Schedule	0.0630	0.0222	2.8364	37	**0.0074**	0.0180	0.1079

Alpha Level 0.05

TABLE 9 (Table 8 Post-Hoc)

Comparing the Ratio of Side Selective Neurons Across all Schedules in M2 ONLY **γ = Ratio of Side Selective Neurons in M2**							
Formula	γ~[1+Schedule+(1|RatID)]						
Coefficients	**β**	SE	tStat	DF	P	CIL	CIU
(Intercept)	0.3033	0.0407	7.4487	16	<0.0001	0.2170	0.3896
Schedule	0.0046	0.0166	0.2758	16	0.7862	-0.0305	0.0397
Comparing the Ratio of Side Selective Neurons Across all Schedules in OFC ONLY **γ = Ratio of Side Selective Neurons in OFC**							
Formula	γ~[1+Schedule+(1|RatID)]						
Coefficients	**β**	SE	tStat	DF	P	CIL	CIU
(Intercept)	0.0658	0.0310	2.1207	22	<0.0001	0.0015	0.1301
Schedule	0.0675	0.0144	4.7031	22	**0.0001**	0.0378	0.0973

Alpha Level 0.05.

TABLE 10

Comparing the Ratio of Outcome Selective Neurons Across all schedules in M2 and OFC **γ = Ratio of Outcome Selective Neurons**							
Formula	γ~[1+Area*Schedule+Session+(1|RatID)]						
Coefficients	**β**	SE	tStat	DF	P	CIL	CIU
(Intercept)	0.4403	0.0906	4.8611	37	<0.0001	0.2568	0.6238
Session	-0.0022	0.0173	-0.1268	37	0.8998	-0.0373	0.0329
Schedule	-0.0893	0.0495	-1.8025	37	0.0796	-0.1896	0.0111
Area	-0.1480	0.0547	-2.7053	37	**0.0103**	-0.2589	-0.0372
Area:Schedule	0.0567	0.0215	2.6416	37	**0.0120**	0.0132	0.1002

Alpha Level 0.05

TABLE 11 (Table 10 Post-Hoc)

Comparing the Ratio of Outcome Selective Neurons Across all Schedules in M2 ONLY **γ = Ratio of Outcome Selective Neurons in M2**							
Formula	γ~[1+Schedule+(1|RatID)]						
Coefficients	**β**	SE	tStat	DF	P	CIL	CIU
(Intercept)	0.2933	0.0365	8.0415	16	<0.0001	0.2160	0.3707
Schedule	-0.0370	0.0169	-2.1900	16	**0.0437**	-0.0728	-0.0012

Comparing the Ratio of Outcome Selective Neurons Across all Schedules in OFC ONLY **γ = Ratio of Outcome Selective Neurons in OFC**							
Formula	γ~[1+Schedule+(1|RatID)]						
Coefficients	**β**	SE	tStat	DF	P	CIL	CIU
(Intercept)	0.1453	0.0386	3.7607	22	0.0011	0.0652	0.2254
Schedule	0.0197	0.0133	1.4809	22	0.1528	-0.0079	0.0473

Alpha Level 0.05.

TABLE 12

Comparing the Ratio of Reward Selective Neurons Across all schedules in M2 and OFC **γ = Ratio of Reward Selective Neurons**							
Formula	γ~[1+Area*Schedule+Session+(1|RatID)]						
Coefficients	**β**	SE	tStat	DF	P	CIL	CIU
(Intercept)	0.7851	0.1869	4.2009	37	0.0002	0.4064	1.1638
Session	0.0018	0.0379	0.0487	37	0.9614	-0.0750	0.0787
Schedule	-0.1200	0.1083	-1.1076	37	0.2752	-0.3394	0.0995
Area	-0.2711	0.1129	-2.4018	37	**0.0215**	-0.4997	-0.0424
Area:Schedule	0.1047	0.0469	2.2316	37	**0.0318**	0.0096	0.1998

Alpha Level 0.05

TABLE 13 (Table 12 Post-Hoc)

Comparing the Ratio of Reward Selective Neurons Across all Schedules in M2 ONLY **γ = Ratio of Reward Selective Neurons in M2**							
Formula	γ~[1+Schedule+(1|RatID)]						
Coefficients	**β**	SE	tStat	DF	P	CIL	CIU
(Intercept)	0.5131	0.0421	12.2008	16	<0.0001	0.4240	0.6023
Schedule	-0.0115	0.0148	-0.7801	16	0.4467	-0.0429	0.0198
Comparing the Ratio of Reward Selective Neurons Across all Schedules in OFC ONLY **γ = Ratio of Reward Selective Neurons in OFC**							
Formula	γ~[1+Schedule+(1|RatID)]						
Coefficients	**β**	SE	tStat	DF	P	CIL	CIU
(Intercept)	0.2421	0.0925	2.6171	22	0.0157	0.0502	0.4339
Schedule	0.0932	0.0391	2.3833	22	**0.0262**	0.0121	0.1743

Alpha Level 0.05.

TABLE 14

Decoder Accuracy modeled by Behavioral Measurements.

γ = Chosen Side Decoder Accuracy

Formula: γ~[1+Session+FlexibilityIndex+PerserverationIndex+InitiationLatency+ChoiceLatency+RewardLatency+WinStay+LoseShift+Area*(Session+FlexibilityIndex+PerserverationIndex+InitiationLatency+ChoiceLatency+RewardLatency+WinStay+LoseShift)+(1|RatID:Session)]

Coefficients	**β**	SE	tStat	DF	P	CIL	CIU
(Intercept)	1.2994	0.4269	3.0436	25	0.0054	0.4201	2.1787
Initiation Latency	-0.0739	0.0653	-1.1326	25	0.2681	-0.2083	0.0605
Choice Latency	0.0264	0.1127	0.2344	25	0.8166	-0.2057	0.2586
Reward Latency	-0.0873	0.0783	-1.1152	25	0.2754	-0.2484	0.0739
WinStay	-1.5011	0.8803	-1.7052	25	0.1006	-3.3140	0.3119
Area	-0.5611	0.2587	-2.1691	25	**0.0398**	-1.0939	-0.0283
LoseShift	-2.2113	1.4948	-1.4793	25	0.1515	-5.2899	0.8673
Flexibility Index	1.1537	0.8096	1.4250	25	0.1665	-0.5137	2.8211
Perseveration Index	3.9990	1.6714	2.3926	25	**0.0246**	0.5566	7.4413
Session	0.0035	0.0099	0.3565	25	0.7244	-0.0168	0.0238
Area:InitiationLatency	0.0608	0.0407	1.4962	25	0.1471	-0.0229	0.1446
Area:ChoiceLatency	-0.0599	0.0841	-0.7127	25	0.4826	-0.2331	0.1132
Area:RewardLatency	0.0242	0.0438	0.5542	25	0.5844	-0.0659	0.1144
Area:Win Stay	1.3807	0.5670	2.4352	25	**0.0224**	0.2130	2.5485
Area:Lose Shift	2.1181	0.9107	2.3258	25	**0.0284**	0.2425	3.9937
Area:Flexibility Index	-0.7755	0.5260	-1.4743	25	0.1529	-1.8589	0.3078
Area:Perseveration Index	-3.9170	1.0290	-3.8066	25	**0.0008**	-6.0363	-1.7978

Alpha Level 0.05

TABLE 15 (Table 14 Post-Hoc)

Post-Hoc Statistics on Area Interaction with M2 Lens Rats only **γ = Chosen Side Decoder Accuracy in M2 Rats**							
Formula	γ~[1+PerseverationIndex+WinStay+LoseShift+(1|RatID:Session)]						
Coefficients	**β**	SE	tStat	DF	P	CIL	CIU
(Intercept)	0.9846	0.1674	5.8818	14	<0.0001	0.6255	1.3436
Win Stay	-0.0131	0.1558	-0.0839	14	0.9343	-0.3472	0.3210
Lose Shift	-0.6778	0.5746	-1.1796	14	0.2578	-1.9102	0.5546
Perseveration Index	-1.0741	0.7841	-1.3699	14	0.1923	-2.7559	0.6076

Post-Hoc Statistics on Area Interaction with OFC Lens Rats only **γ = Chosen Side Decoder Accuracy in OFC Rats**							
Formula	γ~[1+PerseverationIndex+WinStay+LoseShift+(1|RatID:Session)]						
Coefficients	**β**	SE	tStat	DF	P	CIL	CIU
(Intercept)	0.2041	0.1828	1.1167	20	0.2774	-0.1771	0.5853
Win Stay	0.8435	0.2010	4.1975	20	**0.0004**	0.4243	1.2627
Lose Shift	1.4664	0.5304	2.7648	20	**0.0120**	0.3600	2.5729
Perseveration Index	-4.1286	0.6312	-6.5405	20	**<0.0001**	-5.4453	-2.8118

Alpha Level 0.05

TABLE 16

Decoder Accuracy modeled by Behavioral Measurements.
γ = **Trial Outcome Decoder Accuracy**

Formula	γ~[1+Session+FlexibilityIndex+PerserverationIndex+InitiationLatency+ChoiceLatency+RewardLatency+WinStay+LoseShift+Area*(Session+FlexibilityIndex+PerserverationIndex+InitiationLatency+ChoiceLatency+RewardLatency+WinStay+LoseShift)+(1|RatID:Session)]						
Coefficients	**β**	SE	tStat	DF	P	CIL	CIU
Intercept	1.4433	0.4581	3.1505	25	0.0042	0.4998	2.3868
Initiation Latency	-0.1490	0.0700	-2.1278	25	**0.0434**	-0.2932	-0.0048
Choice Latency	0.0677	0.1210	0.5595	25	0.5808	-0.1814	0.3168
Reward Latency	0.1892	0.0840	2.2530	25	**0.0333**	0.0162	0.3621
WinStay	-2.0423	0.9446	-2.1622	25	**0.0404**	-3.9877	-0.0970
Area	-0.7024	0.2776	-2.5304	25	**0.0181**	-1.2741	-0.1307
LoseShift	-2.7002	1.6040	-1.6835	25	0.1047	-6.0037	0.6032
Flexibility Index	0.8666	0.8687	0.9976	25	0.3281	-0.9226	2.6557
Perseveration Index	3.7763	1.7935	2.1056	25	**0.0455**	0.0826	7.4700
Session	0.0087	0.0106	0.8186	25	0.4207	-0.0131	0.0305
Area:InitiationLatency	0.0946	0.0436	2.1676	25	**0.0399**	0.0047	0.1845
Area:ChoiceLatency	-0.0641	0.0902	-0.7109	25	0.4837	-0.2499	0.1217
Area:RewardLatency	-0.0971	0.0469	-2.0688	25	**0.0491**	-0.1938	-0.0004
Area:WinStay	1.5174	0.6084	2.4940	25	**0.0196**	0.2643	2.7704
Area:LoseShift	2.3028	0.9772	2.3565	25	**0.0266**	0.2902	4.3154
Area:Flexibility Index	-0.6076	0.5644	-1.0765	25	0.2920	-1.7701	0.5549
Area:Perseveration Index	-2.4325	1.1041	-2.2031	25	**0.0370**	-4.7065	-0.1585

Alpha Level 0.05

TABLE 17 (Table 16 Post-Hoc)

Post-Hoc Statistics on Area Interaction with M2 Lens Rats only **γ = Trial Outcome Decoder Accuracy in M2 Rats**							
Formula	γ~[1+PerseverationIndex+InitiationLatency+RewardLatency+WinStay+ LoseShift+(1|RatID:Session)]						
Coefficients	**β**	SE	tStat	DF	P	CIL	CIU
(Intercept)	0.8398	0.1998	4.2042	12	0.0012	0.4046	1.2750
Initiation Latency	-0.0678	0.0281	-2.4183	12	**0.0324**	-0.1290	-0.0067
Reward Latency	0.0835	0.0398	2.0961	12	0.0579	-0.0033	0.1703
Win Stay	-0.2921	0.2255	-1.2951	12	0.2197	-0.7834	0.1993
Lose Shift	-0.1878	0.6896	-0.2723	12	0.7901	-1.6903	1.3148
Perseveration Index	0.9463	0.8409	1.1254	12	0.2824	-0.8858	2.7785

Post-Hoc Statistics on Area Interaction with OFC Lens Rats only **γ = Trial Outcome Decoder Accuracy in OFC Rats**							
Formula	γ~[1+PerseverationIndex+InitiationLatency+RewardLatency+WinStay+ LoseShift+(1|RatID:Session)]						
Coefficients	**β**	SE	tStat	DF	P	CIL	CIU
(Intercept)	0.0749	0.1868	0.4007	18	0.6934	-0.3176	0.4674
Initiation Latency	0.0193	0.0151	1.2789	18	0.2172	-0.0124	0.0509
Reward Latency	-0.0069	0.0236	-0.2919	18	0.7737	-0.0564	0.0426
Win Stay	0.6517	0.2268	2.8730	18	**0.0101**	0.1751	1.1283
Lose Shift	1.5504	0.5505	2.8161	18	**0.0114**	0.3937	2.7070
Perseveration Index	-1.5430	0.6310	-2.4452	18	**0.0249**	-2.8687	-0.2172

Alpha Level 0.05

TABLE 18

Across all Blocks in all Sessions for Rats with DREADDs in OFC γ = **Percent Better Option**							
Formula	γ ~ [1 + Drug*Schedule + TrialNum*Block*Session + Sex + (1 + Session*TrialNum*Block | RatID)]						
Coefficients	**β**	SE	tStat	DF	P	CIL	CIU
Intercept	1.0339	0.0569	18.1559	20240	**<0.0001**	0.9222	1.1455
TrialNum	0.0058	0.0006	9.6972	20240	**<0.0001**	0.0046	0.0070
Session	-0.0031	0.0090	-0.3431	20240	0.7315	-0.0208	0.0146
Schedule	-0.0583	0.0022	-26.4746	20240	**<0.0001**	-0.0626	-0.0540
Sex_F	-0.0200	0.0064	-3.1167	20240	**0.0018**	-0.0326	-0.0074
Drug_CNO	-0.0002	0.0061	0.0256	20240	0.9796	-0.0118	0.0121
Block	-0.4084	0.0484	-8.4421	20240	**<0.0001**	-0.5033	-0.3136
TrialNum:Session	-0.0001	0.0001	-1.2576	20240	0.2085	-0.0004	0.0001
Schedule:Drug_CNO	-0.0119	0.0031	3.8331	20240	**0.0001**	0.0058	0.0181
TrialNum:Block	-0.0002	0.0003	-0.6778	20240	0.4979	-0.0009	0.0004
Session:Block	0.0185	0.0050	3.7278	20240	**0.0002**	0.0088	0.0282
TrialNum:Session:Block	<0.0001	<0.0001	-0.5674	20240	0.5705	-0.0001	<0.0001

Alpha Level 0.05

TABLE 19 (Table 18 Post-Hoc)

Post-Hoc Statistics on Schedule Interaction with Schedule 1 Trials only, OFC Rats
γ = **Percent Better Option**

Formula	γ ~ [1 + Drug + Block + TrialNum + Sex + (1 + Block + TrialNum | Rat)]						
Coefficients	**β**	SE	tStat	DF	P	CIL	CIU
(Intercept)	0.9629	0.0232	41.4269	8097	**<0.0001**	0.9173	1.0085
TrialNum	0.0045	0.0002	27.5472	8097	**<0.0001**	0.0042	0.0048
Sex_F	-0.0127	0.0209	-0.6056	8097	0.5448	-0.0537	0.0284
Drug_CNO	-0.0298	0.0036	8.3508	8097	**<0.0001**	0.0228	0.0368
Block	-0.3364	0.0174	-19.3250	8097	**<0.0001**	-0.3705	-0.3022

Post-Hoc Statistics on Schedule Interaction with Schedule 2 Trials only, OFC Rats
γ = **Percent Better Option**

Formula	γ ~ [1 + Drug + Block + TrialNum + Sex + (1 + Block + TrialNum | Rat)]						
Coefficients	**β**	SE	tStat	DF	P	CIL	CIU
(Intercept)	0.9676	0.0292	33.1082	8095	**<0.0001**	0.9103	1.0249
TrialNum	0.0046	0.0003	15.9042	8095	**<0.0001**	0.0041	0.0052
Sex_F	-0.0283	0.0131	-2.1583	8095	0.0309	-0.0540	-0.0026
Drug_CNO	-0.0259	0.0037	7.0715	8095	**<0.0001**	0.0187	0.0330
Block	-0.3541	0.0278	-12.7146	8095	**<0.0001**	-0.4087	-0.2995

Post-Hoc Statistics on Schedule Interaction with Schedule 3 Trials only, OFC Rats
γ = **Percent Better Option**

Formula	γ ~ [1 + Drug + Block + TrialNum + Sex + (1 + Block + TrialNum | Rat)]						
Coefficients	**β**	SE	tStat	DF	P	CIL	CIU
(Intercept)	0.9585	0.0464	20.6677	4045	**<0.0001**	0.8675	1.0494
TrialNum	0.0035	0.0005	7.6799	4045	**<0.0001**	0.0026	0.0044
Sex_F	-0.0193	0.0186	-1.0413	4045	0.2978	-0.0557	0.0171
Drug_CNO	-0.0589	0.0059	9.9401	4045	**<0.0001**	0.0473	0.0706
Block	-0.3420	0.0357	-9.5739	4045	**<0.0001**	-0.4121	-0.2720

Alpha Level 0.05

TABLE 20

Across all Blocks in all Sessions for Rats with DREADDs in M2 γ = **Percent Better Option**							
Formula	γ ~ [1 + Drug*Schedule + TrialNum*Block*Session + Sex + (1 + Session*TrialNum*Block | RatID)]						
Coefficients	**β**	SE	tStat	DF	P	CIL	CIU
Intercept	0.9770	0.0849	11.5025	20238	**<0.0001**	0.8105	1.1434
TrialNum	0.0030	0.0028	1.0969	20238	0.2727	-0.0024	0.0084
Session	-0.0068	0.0176	-0.3873	20238	0.6985	-0.0413	0.0277
Schedule	-0.0076	0.0024	-3.1605	20238	**0.0016**	-0.0123	-0.0029
Sex_M	-0.1370	0.0178	-7.6943	20238	**<0.0001**	-0.1719	-0.1021
Drug_CNO	-0.0501	0.0066	7.5640	20238	**<0.0001**	0.0371	0.0631
Block	-0.3785	0.0742	-5.1017	20238	**<0.0001**	-0.5240	-0.2331
TrialNum:Session	<0.0001	0.0003	0.1577	20238	0.8747	-0.0005	0.0006
Schedule:Drug_CNO	0.0236	0.0034	-6.9678	20238	**<0.0001**	-0.0303	-0.0170
TrialNum:Block	0.0005	0.0010	0.4624	20238	0.6438	-0.0015	0.0024
Session:Block	0.0137	0.0172	0.7986	20238	0.4245	-0.0200	0.0474
TrialNum:Session:Block	-0.0001	0.0001	-0.4427	20238	0.6580	-0.0003	0.0002

Alpha Level 0.05

TABLE 21 (Table 20 Post-Hoc)

Post-Hoc Statistics on Schedule Interaction with Schedule 1 Trials only, M2 Rats γ = **Percent Better Option**							
Formula	γ ~ [1 + Block + Sex + Drug + (1 + Block | RatID)]						
Coefficients	**β**	SE	tStat	DF	P	CIL	CIU
Intercept	0.6215	0.0260	23.9267	8096	**<0.0001**	0.5706	0.6724
Sex_M	0.1082	0.0373	2.8997	8096	**0.0037**	0.0351	0.1814
Drug_CNO	-0.0390	0.0046	8.4151	8096	**<0.0001**	0.0299	0.0481
Block	-0.0067	0.0073	-0.9143	8096	0.3606	-0.0210	0.0076

Post-Hoc Statistics on Schedule Interaction with Schedule 2 Trials only, M2 Rats γ = **Percent Better Option**							
Formula	γ ~ [1 + Block + Sex + Drug + (1 + Block | RatID)]						
Coefficients	**β**	SE	tStat	DF	P	CIL	CIU
Intercept	0.6892	0.0252	27.3697	8096	**<0.0001**	0.6398	0.7385
Sex_M	0.0841	0.0371	2.2682	8096	**0.0233**	0.0114	0.1568
Drug_CNO	-0.0045	0.0045	0.9999	8096	0.3174	-0.0044	0.0134
Block	-0.0237	0.0072	-3.3023	8096	**0.0010**	-0.0377	-0.0096

Post-Hoc Statistics on Schedule Interaction with Schedule 3 Trials only, M2 Rats γ = **Percent Better Option**							
Formula	γ ~ [1 + Block + Sex + Drug + (1 + Block | RatID)]						
Coefficients	**β**	SE	tStat	DF	P	CIL	CIU
Intercept	0.6926	0.0418	16.5647	4046	**<0.0001**	0.6106	0.7745
Sex_M	0.1087	0.0381	2.8559	4046	**0.0043**	0.0341	0.1833
Drug_CNO	0.0046	0.0062	-0.7531	4046	0.4514	-0.0167	0.0074
Block	-0.0551	0.0160	-3.4465	4046	**0.0006**	-0.0864	-0.0238

Alpha Level 0.05

TABLE 22

Across all Blocks in all Sessions for Rats with DREADDs in OFC γ = **Win-Stay**							
Formula	γ ~ [1 + Drug*Schedule + TrialNum*Block*Session + Sex + (1 + Session*TrialNum*Block | RatID)]						
Coefficients	**β**	SE	tStat	DF	P	CIL	CIU
Intercept	0.7508	0.0442	16.9893	20240	**<0.0001**	0.6641	0.8374
TrialNum	0.0076	0.0034	2.2091	20240	**0.0272**	0.0009	0.0144
Session	0.0016	0.0039	0.4146	20240	0.6784	-0.0060	0.0092
Schedule	-0.0944	0.0024	-39.3785	20240	**<0.0001**	-0.0991	-0.0897
Sex_M	-0.0155	0.0097	-1.5975	20240	0.1102	-0.0346	0.0035
Drug_CNO	-0.0201	0.0066	3.0346	20240	**0.0024**	0.0071	0.0331
Block	-0.3234	0.0736	-4.3964	20240	**<0.0001**	-0.4675	-0.1792
TrialNum:Session	-0.0001	0.0005	-0.2566	20240	0.7975	-0.0011	0.0009
Schedule:Drug_CNO	-0.0023	0.0034	0.6819	20240	0.4953	-0.0043	0.0090
TrialNum:Block	-0.0010	0.0018	-0.5441	20240	0.5864	-0.0045	0.0025
Session:Block	0.0191	0.0050	3.8428	20240	**0.0001**	0.0094	0.0288
TrialNum:Session:Block	<0.0001	0.0003	-0.1053	20240	0.9161	-0.0005	0.0005

Alpha Level 0.05

TABLE 23

Across all Blocks in all Sessions for Rats with DREADDs in M2 γ = **Win-Stay**							
Formula	γ ~ [1 + Drug*Schedule + TrialNum*Block*Session + Sex + (1 + Session*TrialNum*Block | RatID)]						
Coefficients	**β**	SE	tStat	DF	P	CIL	CIU
Intercept	0.5342	0.0925	5.7756	20238	**<0.0001**	0.3529	0.7155
TrialNum	0.0040	0.0012	3.2553	20238	**0.0011**	0.0016	0.0065
Session	-0.0075	0.0193	-0.3903	20238	0.6963	-0.0454	0.0303
Schedule	-0.0297	0.0026	-11.4155	20238	**<0.0001**	-0.0348	-0.0246
Sex_M	0.1706	0.0487	3.5053	20238	**0.0005**	0.0752	0.2660
Drug_CNO	-0.0491	0.0072	6.8196	20238	**<0.0001**	0.0350	0.0632
Block	-0.2967	0.0723	-4.1009	20238	**<0.0001**	-0.4385	-0.1549
TrialNum:Session	0.0001	0.0002	0.5287	20238	0.5970	-0.0003	0.0005
Schedule:Drug_CNO	0.0227	0.0037	-6.1528	20238	**<0.0001**	-0.0299	-0.0154
TrialNum:Block	-0.0001	0.0005	-0.1384	20238	0.8900	-0.0010	0.0008
Session:Block	0.0162	0.0144	1.1225	20238	0.2617	-0.0121	0.0445
TrialNum:Session:Block	-0.0001	0.0001	-1.0181	20238	0.3086	-0.0003	0.0001

Alpha Level 0.05

TABLE 24 (Table 23 Post-Hoc)

Post-Hoc Statistics on Schedule Interaction with Schedule 1 Trials only, M2 Rats γ = **Win-Stay**							
Formula	γ ~ [1 + Drug + Block + TrialNum + Sex + (1 + Block + TrialNum | RatID)]						
Coefficients	**β**	SE	tStat	DF	P	CIL	CIU
Intercept	0.5984	0.0446	13.4130	8095	**<0.0001**	0.5110	0.6859
TrialNum	0.0042	0.0004	10.2570	8095	**<0.0001**	0.0034	0.0050
Sex_M	0.0684	0.0457	1.4966	8095	0.1345	-0.0212	0.1581
Drug_CNO	-0.0402	0.0051	7.8506	8095	**<0.0001**	0.0301	0.0502
Block	-0.3124	0.0236	-13.2380	8095	**<0.0001**	-0.3587	-0.2662

Post-Hoc Statistics on Schedule Interaction with Schedule 2 Trials only, M2 Rats γ = **Win-Stay**							
Formula	γ ~ [1 + Drug + Block + TrialNum + Sex + (1 + Block + TrialNum | RatID)]						
Coefficients	**β**	SE	tStat	DF	P	CIL	CIU
Intercept	0.6357	0.0546	11.6450	8095	**<0.0001**	0.5287	0.7427
TrialNum	0.0035	0.0004	10.0400	8095	**<0.0001**	0.0028	0.0042
Sex_M	-0.0229	0.0449	-0.5106	8095	0.6097	-0.1109	0.0650
Drug_CNO	-0.0131	0.0045	2.8746	8095	**0.0041**	0.0042	0.0220
Block	-0.2734	0.0289	-9.4629	8095	**<0.0001**	-0.3301	-0.2168

Post-Hoc Statistics on Schedule Interaction with Schedule 3 Trials only, M2 Rats γ = **Win-Stay**							
Formula	γ ~ [1 + Drug + Block + TrialNum + Sex + (1 + Block + TrialNum | RatID)]						
Coefficients	**β**	SE	tStat	DF	P	CIL	CIU
Intercept	0.5447	0.0504	10.7970	4045	**<0.0001**	0.4458	0.6436
TrialNum	0.0023	0.0004	6.3844	4045	**<0.0001**	0.0016	0.0030
Sex_M	-0.0231	0.0295	-0.7832	4045	0.4336	-0.0811	0.0348
Drug_CNO	0.0036	0.0050	-0.7180	4045	0.4728	-0.0134	0.0062
Block	-0.1894	0.0221	-8.5861	4045	**<0.0001**	-0.2326	-0.1461

Alpha Level 0.05

TABLE 25

Across all Blocks in all Sessions for Rats with DREADDs in OFC γ = **Lose-Shift**							
Formula	γ ~ [1 + Drug*Schedule + TrialNum*Block*Session + Sex + (1 + Session*TrialNum*Block | RatID)]						
Coefficients	**β**	SE	tStat	DF	P	CIL	CIU
Intercept	0.0829	0.0370	2.2409	20240	**0.0250**	0.0104	0.1555
TrialNum	-0.0017	0.0003	-5.3296	20240	**<0.0001**	-0.0024	-0.0011
Session	-0.0026	0.0029	-0.8734	20240	0.3825	-0.0083	0.0032
Schedule	0.0383	0.0013	30.3738	20240	**<0.0001**	0.0358	0.0408
Sex_M	0.0211	0.0168	1.2557	20240	0.2093	-0.0118	0.0540
Drug_CNO	0.0039	0.0035	-1.1151	20240	0.2648	-0.0107	0.0029
Block	0.0672	0.0222	3.0358	20240	**0.0024**	0.0238	0.1107
TrialNum:Session	<0.0001	0.0001	0.2468	20240	0.8051	-0.0002	0.0002
Schedule:Drug_CNO	0.0031	0.0018	-1.7143	20240	0.0865	-0.0066	0.0004
TrialNum:Block	0.0003	0.0001	2.4758	20240	**0.0133**	0.0001	0.0005
Session:Block	-0.0038	0.0017	-2.1453	20240	**0.0319**	-0.0072	-0.0003
TrialNum:Session:Block	<0.0001	<0.0001	0.2968	20240	0.7666	<0.0001	<0.0001

Alpha Level 0.05

TABLE 26

Across all Blocks in all Sessions for Rats with DREADDs in M2 γ = **Lose-Shift**							
Formula	γ ~ [1 + Drug*Schedule + TrialNum*Block*Session + Sex + (1 + Session*TrialNum*Block | RatID)]						
Coefficients	**β**	SE	tStat	DF	P	CIL	CIU
Intercept	0.1578	0.0256	6.1557	20238	**<0.0001**	0.1075	0.2080
TrialNum	-0.0006	0.0019	-0.3444	20238	0.7306	-0.0043	0.0030
Session	0.0003	0.0093	0.0375	20238	0.9701	-0.0178	0.0185
Schedule	0.0137	0.0013	10.6838	20238	**<0.0001**	0.0112	0.0162
Sex_M	-0.0295	0.0137	-2.1564	20238	**0.0311**	-0.0562	-0.0027
Drug_CNO	-0.0042	0.0035	1.1815	20238	0.2374	-0.0028	0.0111
Block	0.0441	0.0254	1.7377	20238	0.0823	-0.0056	0.0939
TrialNum:Session	<0.0001	0.0001	-0.4566	20238	0.6480	-0.0002	0.0001
Schedule:Drug_CNO	0.0037	0.0018	-2.0413	20238	**0.0412**	-0.0072	-0.0001
TrialNum:Block	<0.0001	0.0001	0.2742	20238	0.7840	-0.0002	0.0003
Session:Block	-0.0015	0.0067	-0.2313	20238	0.8171	-0.0146	0.0115
TrialNum:Session:Block	<0.0001	<0.0001	0.3703	20238	0.7112	-0.0001	0.0001

Alpha Level 0.05

TABLE 27 (Table 26 Post-Hoc)

Post-Hoc Statistics on Schedule Interaction with Schedule 1 Trials only, M2 Rats γ = **Lose-Shift**							
Formula	γ ~ [1 + Drug + Sex + (1 | RatID)]						
Coefficients	**β**	SE	tStat	DF	P	CIL	CIU
Intercept	0.1924	0.0122	15.7972	8097	**<0.0001**	0.1685	0.2163
Sex_M	-0.0499	0.0182	-2.7406	8097	**0.0061**	-0.0856	-0.0142
Drug_CNO	-0.0002	0.0020	0.1118	8097	0.9110	-0.0038	0.0042

Post-Hoc Statistics on Schedule Interaction with Schedule 2 Trials only, M2 Rats γ = **Lose-Shift**							
Formula	γ ~ [1 + Drug + Sex + (1 | RatID)]						
Coefficients	**β**	SE	tStat	DF	P	CIL	CIU
Intercept	0.1956	0.0133	14.7101	8097	**<0.0001**	0.1695	0.2217
Sex_M	-0.0301	0.0199	-1.5155	8097	0.1297	-0.0691	0.0088
Drug_CNO	0.0114	0.0023	-4.9467	8097	**<0.0001**	-0.0159	-0.0069

Post-Hoc Statistics on Schedule Interaction with Schedule 3 Trials only, M2 Rats γ = **Lose-Shift**							
Formula	γ ~ [1 + Drug + Sex + (1 | RatID)]						
Coefficients	**β**	SE	tStat	DF	P	CIL	CIU
Intercept	0.2031	0.0177	11.4884	4047	**<0.0001**	0.1684	0.2377
Sex_M	-0.0111	0.0264	-0.4196	4047	0.6748	-0.0628	0.0407
Drug_CNO	0.0045	0.0033	-1.3500	4047	0.1771	-0.0110	0.0020

Alpha Level 0.05

TABLE 28

Across all Blocks in all Sessions for Rats with DREADDs in OFC γ = **Initiation Latency**							
Formula	γ ~ [1 + Drug*Schedule + TrialNum*Block*Session + Sex + (1 + Session*TrialNum*Block | RatID)]						
Coefficients	**β**	SE	tStat	DF	P	CIL	CIU
Intercept	2.6959	1.0234	2.6343	20240	**0.0084**	0.6900	4.7019
TrialNum	-0.0050	0.0107	-0.4654	20240	0.6416	-0.0259	0.0159
Session	0.0132	0.2386	0.0555	20240	0.9558	-0.4545	0.4809
Schedule	0.3057	0.0726	4.2111	20240	**<0.0001**	0.1634	0.4481
Sex_F	0.8811	0.3127	2.8173	20240	**0.0048**	0.2681	1.4941
Drug_CNO	-0.5554	0.2006	2.7682	20240	**0.0056**	0.1621	0.9486
Block	0.9305	2.1666	0.4295	20240	0.6676	-3.3162	5.1772
TrialNum:Session	-0.0012	0.0050	-0.2347	20240	0.8144	-0.0111	0.0087
Schedule:Drug_CNO	-0.0517	0.1027	0.5034	20240	0.6147	-0.1496	0.2530
TrialNum:Block	0.0002	0.0153	0.0139	20240	0.9889	-0.0297	0.0302
Session:Block	-0.1437	0.1077	-1.3338	20240	0.1823	-0.3548	0.0675
TrialNum:Session:Block	0.0008	0.0023	0.3243	20240	0.7457	-0.0038	0.0053

Alpha Level 0.05

TABLE 29

Across all Blocks in all Sessions for Rats with DREADDs in M2 γ = **Initiation Latency**							
Formula	γ ~ [1 + Drug*Schedule + TrialNum*Block*Session + Sex + (1 + Session*TrialNum*Block | RatID)]						
Coefficients	**β**	SE	tStat	DF	P	CIL	CIU
Intercept	**3.6447**	**0.4890**	**7.4530**	**20238**	**<0.0001**	**2.6862**	**4.6033**
TrialNum	0.0030	0.0156	0.1910	20238	0.8486	-0.0276	0.0336
Session	-0.0144	0.2332	-0.0618	20238	0.9507	-0.4714	0.4426
Schedule	0.0769	0.0692	1.1110	20238	0.2666	-0.0587	0.2125
Sex_M	-0.1767	0.4045	-0.4369	20238	0.6622	-0.9697	0.6162
Drug_CNO	0.0011	0.1912	-0.0058	20238	0.9954	-0.3758	0.3736
Block	0.0697	0.3815	0.1826	20238	0.8551	-0.6781	0.8174
TrialNum:Session	-0.0027	0.0024	-1.1159	20238	0.2645	-0.0074	0.0020
Schedule:Drug_CNO	**-0.3358**	**0.0978**	**3.4323**	**20238**	**0.0006**	**0.1440**	**0.5276**
TrialNum:Block	0.0012	0.0034	0.3496	20238	0.7266	-0.0054	0.0078
Session:Block	<0.0001	0.0683	0.0002	20238	0.9998	-0.1339	0.1339
TrialNum:Session:Block	0.0007	0.0006	1.2140	20238	0.2248	-0.0004	0.0019

Alpha Level 0.05

TABLE 30 (Table 29 Post-Hoc)

Post-Hoc Statistics on Schedule Interaction with Schedule 1 Trials only, M2 Rats γ = **Initiation Latency**							
Formula	γ ~ [1 + Drug + (1 | RatID)]						
Coefficients	**β**	SE	tStat	DF	P	CIL	CIU
Intercept	3.6896	0.4340	8.5022	8098	**<0.0001**	2.8389	4.5403
Drug_CNO	-0.3136	0.1155	2.7158	8098	**0.0066**	0.0872	0.5399

Post-Hoc Statistics on Schedule Interaction with Schedule 2 Trials only, M2 Rats γ = **Initiation Latency**							
Formula	γ ~ [1 + Drug + (1 | RatID)]						
Coefficients	**β**	SE	tStat	DF	P	CIL	CIU
Intercept	4.2507	0.5878	7.2311	8098	**<0.0001**	3.0984	5.4030
Drug_CNO	-0.3586	0.1183	3.0307	8098	**0.0024**	0.1266	0.5905

Post-Hoc Statistics on Schedule Interaction with Schedule 3 Trials only, M2 Rats γ = **Initiation Latency**							
Formula	γ ~ [1 + Drug + (1 | RatID)]						
Coefficients	**β**	SE	tStat	DF	P	CIL	CIU
Intercept	3.6824	0.5522	6.6687	4048	**<0.0001**	2.5998	4.7650
Drug_CNO	-1.0817	0.1631	6.6307	4048	**<0.0001**	0.7619	1.4015

Alpha Level 0.05

TABLE 31

Across all Blocks in all Sessions for Rats with DREADDs in OFC γ = **Choice Latency**							
Formula	γ ~ [1 + Drug*Schedule + TrialNum*Block*Session + Sex + (1 + Session*TrialNum*Block | RatID)]						
Coefficients	**β**	SE	tStat	DF	P	CIL	CIU
Intercept	1.3804	0.1929	7.1550	20240	**<0.0001**	1.0023	1.7586
TrialNum	-0.0094	0.0027	-3.5503	20240	**0.0004**	-0.0146	-0.0042
Session	0.0074	0.0745	0.0989	20240	0.9212	-0.1386	0.1533
Schedule	0.0016	0.0271	0.0597	20240	0.9524	-0.0515	0.0548
Sex_F	0.0683	0.1389	0.4915	20240	0.6230	-0.2040	0.3405
Drug_CNO	0.2487	0.0749	-3.3202	20240	**0.0009**	-0.3955	-0.1019
Block	0.5931	0.1973	3.0068	20240	**0.0026**	0.2065	0.9797
TrialNum:Session	0.0005	0.0005	1.0702	20240	0.2846	-0.0004	0.0015
Schedule:Drug_CNO	-0.1231	0.0383	3.2114	20240	**0.0013**	0.0480	0.1983
TrialNum:Block	0.0009	0.0012	0.7665	20240	0.4434	-0.0014	0.0032
Session:Block	-0.0660	0.0248	-2.6562	20240	**0.0079**	-0.1146	-0.0173
TrialNum:Session:Block	<0.0001	0.0003	0.0710	20240	0.9434	-0.0005	0.0005

Alpha Level 0.05

TABLE 32 (Table 31 Post-Hoc)

Post-Hoc Statistics on Schedule Interaction with Schedule 1 Trials only, OFC Rats γ = **Choice Latency**							
Formula	γ ~ [1 + Drug + Block + Trial + (1 + Block + Trial | RatID)]						
Coefficients	**β**	SE	tStat	DF	P	CIL	CIU
Intercept	1.2756	0.1289	9.8925	8098	**<0.0001**	1.0228	1.5284
TrialNum	-0.0052	0.0022	-2.3588	8098	**0.0184**	-0.0095	-0.0009
Drug_CNO	0.1338	0.0462	-2.8990	8098	**0.0038**	-0.2243	-0.0433
Block	0.4059	0.1247	3.2559	8098	**0.0011**	0.1615	0.6502

Post-Hoc Statistics on Schedule Interaction with Schedule 2 Trials only, OFC Rats γ = **Choice Latency**							
Formula	γ ~ [1 + Drug + Block + Trial + (1 + Block + Trial | RatID)]						
Coefficients	**β**	SE	tStat	DF	P	CIL	CIU
Intercept	1.3616	0.2211	6.1587	8096	**<0.0001**	0.9282	1.7949
TrialNum	-0.0052	0.0015	-3.3657	8096	**0.0008**	-0.0082	-0.0022
Drug_CNO	0.1668	0.0407	-4.1036	8096	**<0.0001**	-0.2465	-0.0871
Block	0.3409	0.0819	4.1620	8096	**<0.0001**	0.1803	0.5014

Post-Hoc Statistics on Schedule Interaction with Schedule 3 Trials only, OFC Rats γ = **Choice Latency**							
Formula	γ ~ [1 + Drug + Block + Trial + (1 + Block + Trial | RatID)]						
Coefficients	**β**	SE	tStat	DF	P	CIL	CIU
Intercept	1.3046	0.2529	5.1596	4046	**<0.0001**	0.8089	1.8004
TrialNum	-0.0022	0.0018	-1.1894	4046	0.2344	-0.0058	0.0014
Drug_CNO	-0.1649	0.0741	2.2252	4046	**0.0261**	0.0196	0.3103
Block	0.2284	0.1436	1.5900	4046	0.1119	-0.0532	0.5099

Alpha Level 0.05

TABLE 33

Across all Blocks in all Sessions for Rats with DREADDs in M2 γ = **Choice Latency**							
Formula	γ ~ [1 + Drug*Schedule + TrialNum*Block*Session + Sex + (1 + Session*TrialNum*Block | RatID)]						
Coefficients	**β**	SE	tStat	DF	P	CIL	CIU
Intercept	0.6755	0.1966	3.4364	20238	**0.0006**	0.2902	1.0608
TrialNum	-0.0051	0.0025	-2.0942	20238	**0.0363**	-0.0100	-0.0003
Session	0.1483	0.0633	2.3435	20238	**0.0191**	0.0243	0.2723
Schedule	0.1097	0.0276	3.9773	20238	**0.0001**	0.0557	0.1638
Sex_M	0.0199	0.1316	0.1509	20238	0.8800	-0.2380	0.2777
Drug_CNO	0.1377	0.0762	-1.8059	20238	0.0709	-0.2871	0.0118
Block	0.4703	0.1530	3.0742	20238	**0.0021**	0.1704	0.7701
TrialNum:Session	-0.0003	0.0006	-0.5802	20238	0.5618	-0.0014	0.0008
Schedule:Drug_CNO	-0.1154	0.0390	2.9586	20238	**0.0031**	0.0390	0.1919
TrialNum:Block	0.0001	0.0010	0.1205	20238	0.9041	-0.0018	0.0020
Session:Block	-0.0797	0.0326	-2.4419	20238	**0.0146**	-0.1437	-0.0157
TrialNum:Session:Block	0.0003	0.0003	1.2074	20238	0.2273	-0.0002	0.0009

Alpha Level 0.05

TABLE 34 (Table 33 Post-Hoc)

Post-Hoc Statistics on Schedule Interaction with Schedule 1 Trials only, M2 Rats γ = **Choice Latency**							
Formula	γ ~ [1 + Drug + Block + Trial + (1 + Block + Trial | RatID)]						
Coefficients	**β**	SE	tStat	DF	P	CIL	CIU
Intercept	1.1142	0.0962	11.5848	8096	**<0.0001**	0.9257	1.3028
TrialNum	-0.0049	0.0014	-3.5898	8096	**0.0003**	-0.0076	-0.0022
Drug_CNO	0.0325	0.0431	-0.7526	8096	0.4517	-0.1170	0.0521
Block	0.4320	0.1160	3.7240	8096	**0.0002**	0.2046	0.6594

Post-Hoc Statistics on Schedule Interaction with Schedule 2 Trials only, M2 Rats γ = **Choice Latency**							
Formula	γ ~ [1 + Drug + Block + Trial + (1 + Block + Trial | RatID)]						
Coefficients	**β**	SE	tStat	DF	P	CIL	CIU
Intercept	1.3058	0.1501	8.6983	8096	**<0.0001**	1.0115	1.6000
TrialNum	-0.0009	0.0017	-0.5260	8096	0.5989	-0.0043	0.0025
Drug_CNO	-0.2460	0.0478	5.1465	8096	**<0.0001**	0.1523	0.3397
Block	0.1350	0.0917	1.4723	8096	0.1410	-0.0448	0.3148

Post-Hoc Statistics on Schedule Interaction with Schedule 3 Trials only, M2 Rats γ = **Choice Latency**							
Formula	γ ~ [1 + Drug + Block + Trial + (1 + Block + Trial | RatID)]						
Coefficients	**β**	SE	tStat	DF	P	CIL	CIU
Intercept	1.8224	0.4107	4.4377	4046	**<0.0001**	1.0173	2.6276
TrialNum	-0.0038	0.0020	-1.8416	4046	0.0656	-0.0078	0.0002
Drug_CNO	-0.1439	0.0687	2.0959	4046	**0.0362**	0.0093	0.2786
Block	0.1336	0.1502	0.8895	4046	0.3738	-0.1609	0.4282

Alpha Level 0.05

TABLE 35

Across all Blocks in all Sessions for Rats with DREADDs in OFC γ = **Reward Latency**							
Formula	γ ~ [1 + Drug*Schedule + TrialNum*Block*Session + Sex + (1 + Session*TrialNum*Block | RatID)]						
Coefficients	**β**	SE	tStat	DF	P	CIL	CIU
Intercept	2.1261	0.2672	7.9569	14690	**<0.0001**	1.6023	2.6498
TrialNum	0.0019	0.0029	0.6403	14690	0.5220	-0.0038	0.0076
Session	-0.0333	0.0395	-0.8441	14690	0.3986	-0.1107	0.0441
Schedule	0.0017	0.0383	0.0440	14690	0.9649	-0.0734	0.0767
Sex_F	0.2390	0.1168	2.0464	14690	**0.0407**	0.0101	0.4680
Drug_CNO	0.3113	0.1006	-3.0941	14690	**0.0020**	-0.5086	-0.1141
Block	-0.3349	0.2282	-1.4674	14690	0.1423	-0.7823	0.1125
TrialNum:Session	0.0009	0.0005	1.7064	14690	0.0880	-0.0001	0.0019
Schedule:Drug_CNO	-0.0497	0.0536	0.9285	14690	0.3532	-0.0553	0.1547
TrialNum:Block	0.0015	0.0012	1.2878	14690	0.1978	-0.0008	0.0038
Session:Block	0.0698	0.0411	1.6998	14690	0.0892	-0.0107	0.1503
TrialNum:Session:Block	-0.0006	0.0002	-2.4445	14690	**0.0145**	-0.0011	-0.0001

Alpha Level 0.05

TABLE 36

Across all Blocks in all Sessions for Rats with DREADDs in M2 γ = **Reward Latency**							
Formula	γ ~ [1 + Drug*Schedule + TrialNum*Block*Session + Sex + (1 + Session*TrialNum*Block | RatID)]						
Coefficients	**β**	SE	tStat	DF	P	CIL	CIU
(Intercept)	0.5881	0.2684	2.1912	12522	**0.0285**	0.0620	1.1142
TrialNum	0.0018	0.0009	1.9920	12522	**0.0464**	<0.0001	0.0036
Session	0.0446	0.0394	1.1300	12522	0.2585	-0.0327	0.1219
Schedule	0.1046	0.0116	9.0526	12522	**<0.0001**	0.0820	0.1273
Sex_M	0.9225	0.1462	6.3112	12522	**<0.0001**	0.6360	1.2090
Drug_CNO	-0.1902	0.0309	6.1626	12522	**<0.0001**	0.1297	0.2507
Block	0.2866	0.1360	2.1071	12522	**0.0351**	0.0200	0.5532
TrialNum:Session	-0.0001	0.0002	-0.8107	12522	0.4176	-0.0005	0.0002
Schedule:Drug_CNO	0.0871	0.0162	-5.3764	12522	**<0.0001**	-0.1189	-0.0554
TrialNum:Block	-0.0011	0.0008	-1.5102	12522	0.1310	-0.0026	0.0003
Session:Block	-0.0421	0.0153	-2.7478	12522	**0.0060**	-0.0721	-0.0121
TrialNum:Session:Block	0.0001	0.0001	1.5855	12522	0.1129	<0.0001	0.0003

Alpha Level 0.05

TABLE 37 (Table 36 Post-Hoc)

Post-Hoc Statistics on Schedule Interaction with Schedule 1 Trials only, M2 Rats
γ = **Reward Latency**

Formula	γ ~ [1 + Drug + TrialNum + Block + Sex + (1 + TrialNum + Block | RatID)]						
Coefficients	**β**	SE	tStat	DF	P	CIL	CIU
(Intercept)	1.1237	0.1478	7.6030	5320	**<0.0001**	0.8340	1.4135
TrialNum	-0.0011	0.0008	-1.3713	5320	0.1703	-0.0026	0.0005
Sex_M	0.2739	0.2184	1.2546	5320	0.2097	-0.1541	0.7020
Drug_CNO	-0.1507	0.0187	8.0430	5320	**<0.0001**	0.1140	0.1875
Block	0.1674	0.0569	2.9406	5320	**0.0033**	0.0558	0.2790

Post-Hoc Statistics on Schedule Interaction with Schedule 2 Trials only, M2 Rats
γ = **Reward Latency**

Formula	γ ~ [1 + Drug + TrialNum + Block + Sex + (1 + TrialNum + Block | RatID)]						
Coefficients	**β**	SE	tStat	DF	P	CIL	CIU
(Intercept)	1.6060	0.1800	8.9232	4991	**<0.0001**	1.2532	1.9589
TrialNum	0.0010	0.0007	1.4326	4991	0.1520	-0.0004	0.0023
Sex_M	0.1288	0.1685	0.7641	4991	0.4449	-0.2016	0.4592
Drug_CNO	0.0938	0.0177	-5.2970	4991	**<0.0001**	-0.1285	-0.0591
Block	-0.0612	0.0580	-1.0566	4991	0.2907	-0.1749	0.0524

Post-Hoc Statistics on Schedule Interaction with Schedule 3 Trials only, M2 Rats
γ = **Reward Latency**

Formula	γ ~ [1 + Drug + TrialNum + Block + Sex + (1 + TrialNum + Block | RatID)]						
Coefficients	**β**	SE	tStat	DF	P	CIL	CIU
(Intercept)	1.5501	0.1547	10.0185	2208	**<0.0001**	1.2467	1.8536
TrialNum	0.0017	0.0012	1.3656	2208	0.1722	-0.0007	0.0040
Sex_M	0.3522	0.2061	1.7086	2208	0.0877	-0.0520	0.7565
Drug_CNO	-0.0228	0.0343	0.6637	2208	0.5070	-0.0445	0.0900
Block	-0.1449	0.0691	-2.0977	2208	**0.0360**	-0.2805	-0.0094

Alpha Level 0.05